Integrated Solar Absorption Cooling and Membrane Distillation Systems – A Theoretical Study

BY

AHMED YASSEN

A Thesis Presented to the

DEANSHIP OF GRADUATE STUDIES

KING FAHD UNIVERSITY OF PETROLEUM & MINERALS

DHAHRAN, SAUDI ARABIA

In Partial Fulfillment of the
Requirements for the Degree of

MASTER OF SCIENCE

In

MECHANICAL ENGINEERING

December, 2016

KING FAHD UNIVERSITY OF PETROLEUM & MINERALS

DHAHRAN- 31261, SAUDI ARABIA

DEANSHIP OF GRADUATE STUDIES

This thesis, written by **AHMED SALAH MOHAMED YASSEN** under the direction of his thesis advisor and approved by his thesis committee, has been presented and accepted by the Dean of Graduate Studies, in partial fulfillment of the requirements for the degree of **MASTER OF SCIENCE IN MECHANICAL ENGINEERING.**

Dr. Mohammed A. Antar

(Advisor)

Dr. Zuhair M. A. Gasem

Department Chairman

Dr. Syed A. M. Said

(Member)

Dr. Salam A. Zummo

Dean of Graduate Studies

Dr. Atia E. Khalifa

(Member)

19/1/17

Date

In the name of Allah, the most Gracious and the most Merciful

Dedicated to

My Beloved Parents

My Only Sister

My Brothers

ACKNOWLEDGMENTS

This research work would not have been possible without the help of Allah Almighty, who kept me focused and provided me with sound health and wellbeing towards the successful completion of my MS thesis. I am grateful to my mother who is my beacon of light in the most difficult times and who supported my decision to join KFUPM.

I acknowledge, with deep gratitude and appreciation, my previous advisor Dr. Maged I. El-Shaarawi for his valuable guidance, enlightening ideas and encouragement towards my thesis work. His motivation, and immense knowledge was indeed the help I needed to achieve my goals. I really enjoyed the time I spent working with him, but, regrettably, due to some health matters that he encountered, this period was cut short and he had to resign from the university, I truly wish he feels better soon, and may Allah bless him.

Special thanks to my advisor, Dr. Mohammed A. Antar, for his continuous guidance, supervision and for taking it upon him to continue the work of my previous advisor, I'm indebted for his support. I would also like to thank, Dr. S. A. M. Said and Dr. Atia Khalifa for their motivation and valuable time and effort that they dedicated on my research.

Deep gratitude is also due to my distinguished friends in KFUPM, Mujahid Omer, Marwan Nagm Eldeen, Hamza Mukhtar, Suhaib Mustafa, Mozamil Khalid and Mohamed Abdelwahab for making my stay at KFUPM a memorable journey of my life. I also would like to thank my brothers and my sister for their prayers and moral support throughout my academic life and for filling my life with joy and happiness. My acknowledgement is also due to KFUPM for granting me the opportunity to pursue my graduate studies.

TABLE OF CONTENTS

LIST OF TABLES

LIST OF FIGURES

LIST OF SYMBOLES AND ABBREVIATIONS

COP	:	Coefficient of performance
W	:	Solution pump work, W
W	:	Work, W
I	:	Daily solar radiation, kWh/m^2
h	:	Enthalpy, kJ/kg
$\dot{m}$	:	Mass flow rate, kg/s
P_{high}	:	High-side pressure, kPa
P_{low}	:	Low-side pressure, kPa
ΔP	:	Pressure difference, Pa
$\dot{Q}$	:	Heat transfer rate, W
T	:	Temperature, ºC
$LMTD$	:	Log-mean temperature difference, ºC
X	:	Concentration of lithium bromide
A	:	Area, m^2
C_p	:	Specific Heat, J/kg-K
D_h	:	Hydraulic Diameter, m
d_{pore}	:	Pore Diameter, m
D_e	:	Diffusion Coefficient, m^2/s
h_f	:	Convective Heat Transfer Coefficient of feed side, W/m^2-K
h_p	:	Convective Heat Transfer Coefficient of permeate side, W/m^2-K

ΔH	:	Enthalpy or Latent Heat of vaporization of water, kJ/kg
k	:	Thermal Conductivity, W/m-K
M	:	Molecular Weight, g/mol
J_w	:	Mass Flux, kg/m^2-s
p	:	Pressure, Pa
R	:	Universal gas constant, 8314 J/kmol-K
Nu	:	Nusselt number
Re	:	Reynolds number
Pr	:	Prandtl number
U	:	Overall heat transfer coefficient, W/m^2-K
x	:	Mole Fraction
L	:	Length, m

Abbreviations

DCMD	:	Direct Contact Membrane Distillation
SGMD	:	Sweep Gas Membrane Distillation
VMD	:	Vacuum Membrane Distillation
AGMD	:	Air Gap Membrane Distillation

Greek Symbols

η	:	Efficiency
υ	:	Specific volume
α	:	Contribution of knudsen diffusion to mass transfer
δ	:	Membrane Thickness, m

ε	:	Porosity, %
μ	:	Viscosity, Pa-s
γ	:	Salt activity coefficient
τ	:	Membrane Tortuosity

Subscripts

ss	:	Strong Solution
ws	:	Weak Solution
r	:	Refrigerant
g	:	Generator
a	:	Absorber
c	:	Condenser
e	:	Evaporator
f	:	Feed side
p	:	Permeate side
bf	:	Bulk Feed
bp	:	Bulk Permeate
mf	:	Membrane Feed Surface
mp	:	Membrane permeate Surface
m	:	Mean or Average Property
k	:	Knudsen
v	:	Vapors/ Vaporization
w	:	Water
w,a	:	Water in Air

ABSTRACT

Full Name : **[Ahmed Salah Mohamed Yassen]**

Thesis Title : **[Integrated Solar Absorption Cooling and Membrane Distillation Systems – A Theoretical Study]**

Major Field : **[Mechanical Engineering]**

Date of Degree : **[December, 2016]**

Hot climate and water scarcity are the most predominant problems in different regions all over the world, especially in the Gulf Co-operating Countries (GCC). These problems have to be solved in efficient and sustainable way to sustain the life in these countries. Several types of solar air conditioning and thermal water desalination systems have been used for individual air conditioning and water desalination applications. Few researchers have addressed the concept of air conditioning and water desalination cogeneration that aim to simultaneously producing cooling effect and desalinated water. This integration can achieve high technical as well as economic benefits. In this thesis, an innovative system of combined solar absorption cooling cycle and thermal membrane distillation (MD) unit were adopted. The proposed system is composed of a single effect lithium bromide-water absorption refrigeration cycle which utilizes solar energy as the heat source and a direct contact membrane distillation unit where the hot feed and the cold permeate required by the MD unit are supplied from the absorption cooling system.

The main objective of the proposed system is to simultaneously produce cooling effect and fresh water for a typical family house in Saudi Arabia. Several configurations; (A), (B) and (C), were developed to improve the performance of the MD system by increasing the

desalination yield. In all arrangements, the feed side of DCMD unit is driven by the heat rejected from the absorption system. Configuration (A) utilizes the cooling seawater for the cold side of DCMD unit while configuration (B) and (C) share the chilled water produced from the absorption system with partial cooling load requirements (Configuration B) or no cooling load (configuration C) where all the cooling effect is forwarded to the DCMD system. The results show that configuration (A) for the proposed integrated system is the best choice for providing a cooling effect, then followed by configuration (B) with 25 %, 50 % and 75 % partial cooling load and the rest is bypassed to DCMD system with maximum cooling effect obtained as 26, 19.5, 9.8 and 2.5 kW, respectively. In addition, configuration (C) appears to have the best performance in term of water productivity that can reach up to 140 kg/m^2-hr compared to 133, 125, 118 and 110 for configuration (B) with 75 %, 50 %, 25 % and configuration (A), respectively.

ملخص الرسالة

الاسم الكامل	:	**أحمد صلاح محمد يس**
عنوان الرسالة	:	**الأنظمة المزدوجة للتبريد الإمتصاصي بالطاقة الشمسية مع التقطير بإستخدام غشاء**
التخصص	:	**الهندسة الميكانيكية**
تاريخ الدرجة العلمية	:	**ديسمبر- 2016**

المناخ الحار وندرة المياه هي من أكثر المشاكل السائدة في مناطق مختلفة في جميع أنحاء العالم، وخصوصاً في منطقة الخليج. هذه المشاكل يجب أن تحل بطريقة فعالة ومستدامة للحفاظ على الحياة في تلك البلدان. عدة أنواع من أنظمة تكييف الهواء التي تعمل بالطاقة الشمسية وأنظمة تحلية المياه الحرارية قد أستخدمت في التطبيقات المنفصلة لتكييف الهواء وتحلية المياه. عدد قليل من الباحثين تناولو مفهوم الربط بين عمليات تكييف الهواء وتحلية المياه والذي يهدف إلى الإنتاج المتزامن للأثر التبريدي والمياه المحلاة. هذا التكامل يمكن أن يحقق فوائد تقنية عالية بالإضافة الي فوائد إقتصادية. في هذه الأطروحة، تم تطوير نظام مبتكر والذي يربط دورة التبريد الإمتصاصية التي تعمل بالطاقة الشمسية ووحدة تحلية مياه بإستخدام غشاء. يتكون النظام المقترح من دورة التبريد الإمتصاصية أحادية التأثير والتي تستخدم خليط بروميد الليثيوم والماء وتستمد طاقة عملها من الطاقة الشمسية ووحدة إتصال مباشر لتحلية المياه بإستخدام غشاء والتي تستمد الماء البارد والساخن من دورة التبريد التبريد الإمتصاصية.

يهدف النظام المقترح الي الإنتاج المتزامن للأثر التبريدي والمياه المحلاة لنموذج منزل عائلي في المملكة العربية السعودية. تم إبتكار عدد من التصاميم، التصميم (A) و(B) و(C)، والتي تهدف إلي تحسين أداء نظام تحلية المياه عن طريق زيادة معدل إنتاج المياه المحلاة. في جميع التصاميم، تتم تغذية الجزء الساخن لوحدة تحلية المياه بواسطة الحرارة المطرودة من نظام التبريد الإمتصاصي. التصميم (A) يستخدم مياه البحر لزيادة البرودة في الجانب البارد لوحدة تحلية المياه بينما التصميم (B) و(C) يستخدم جزء من المياه المبردة التي تنتج من نظام التبريد الإمتصاصي بالنسبة للتصميم (B) بينما لا يوجد حمل تبريد للتصميم (C) ويتم إستخدام المياه المبردة كلها في وحدة تحلية المياه. وقد أظهرت النتائج

أن التصميم (A) للنظام المتكامل المقترح هو الخيار الأفضل لتوفير الأثر التبريدي، ثم يليه التصميم (B) بنسب إلتفافيه 25٪ و50٪ و75٪ مع أكبر قدر من الأثر التبريدي الذي يمكن الحصول عليه حيث يقدر بنحو 26، 19.5و 9.8 و 2.5 كيلو واط، على التوالي. بالإضافة إلى ذلك، وجد أن التصميم (C) هو الأفضل أداءً من حيث إنتاجية المياه التي يمكن أن تصل إلى 140 كجم/متر^2-ساعة مقارنة ب133 و125 و118 و110 للتصميم (B) بنسب إلتفافيه 75٪، 50٪، 25٪ والتصميم (A)، على التوالي.

CHAPTER 1

INTRODUCTION

1.1 Overview

The Kingdom of Saudi Arabia is one of the fastest growing consumer of energy. Nowadays, the relatively high hot summer temperatures and water shortage are two major problems facing the Kingdom. These problems lead to a rapidly increase in the rate of energy consumption for both fresh water production and air-conditioning in building sector. Both commercial and residential sectors are facing this challenge and it will keep rising up in the future with the population growth and the improvements in the standard of living. Presently, vapor compression systems are almost producing all the cooling required in the Kingdom. The production of the cooling for air-conditioning purposes is usually consuming large amount of electrical energy which is generally obtained by burning fossil fuel. Furthermore, the air conditioning systems which already excited in buildings are consuming about 65% of the overall electric energy generated in the Kingdom. Another important proportion of these energy is dedicated to satisfy fresh water needs [1]. For the time being, the water scarcity problem has been partially solved by desalinating seawater which consumes large quantities of thermal or mechanical energy and has a negative effect on the environment.

Due to worldwide consciousness of energy problems, renewable sources of energy should be considered in the design of fresh water production facilities. Solar energy emerges as the most promising one out of these sources. Thus, solar energy should be primarily used to produce the required fresh water and to provide the necessary comfort conditions. On the other hand, employing solar energy for creating human comfort conditions can be achieved by using solar powered absorption cooling units. Therefore, the machinery and large amount of electrical energy required for vapor compression units can be avoided. Therefore, new innovative technologies are required for water production and air-conditioning that will significantly share the load generated by one of the renewable energy sources.

1.2 Solar Absorption Refrigeration System

Absorption cycles have been employed in refrigeration for many years, but have attracted renewed interest in recent years due to environmental concerns related to global warming. Most absorption systems use working fluids that have extremely low global warming potential (GWP) values compared to conventional refrigerants such as hydro-chloro-fluoro-carbons (HCFC). Furthermore, the ability to utilize waste heat as the input energy in these thermally driven systems for space conditioning and refrigeration applications can lead to increased energy savings.

Vapor-compression heat pumps operate by circulating a refrigerant between low and high pressure sides, removing heat from a low temperature source and rejecting heat to a high temperature sink. Figure 1.1 shows a schematic of a simple vapor-compression heat pump. Low pressure refrigerant vapor enters the compressor where it is compressed to a high pressure by work input. It then enters the condenser where it condenses, rejecting its latent

heat to the hot ambient. The refrigerant leaves the condenser as a subcooled liquid before it flows through an expansion valve to a lower pressure. Subsequently, the refrigerant enters the evaporator where it acquires heat from the conditioned space to provide the desired cooling. Once the refrigerant is completely evaporated, it returns to the compressor.

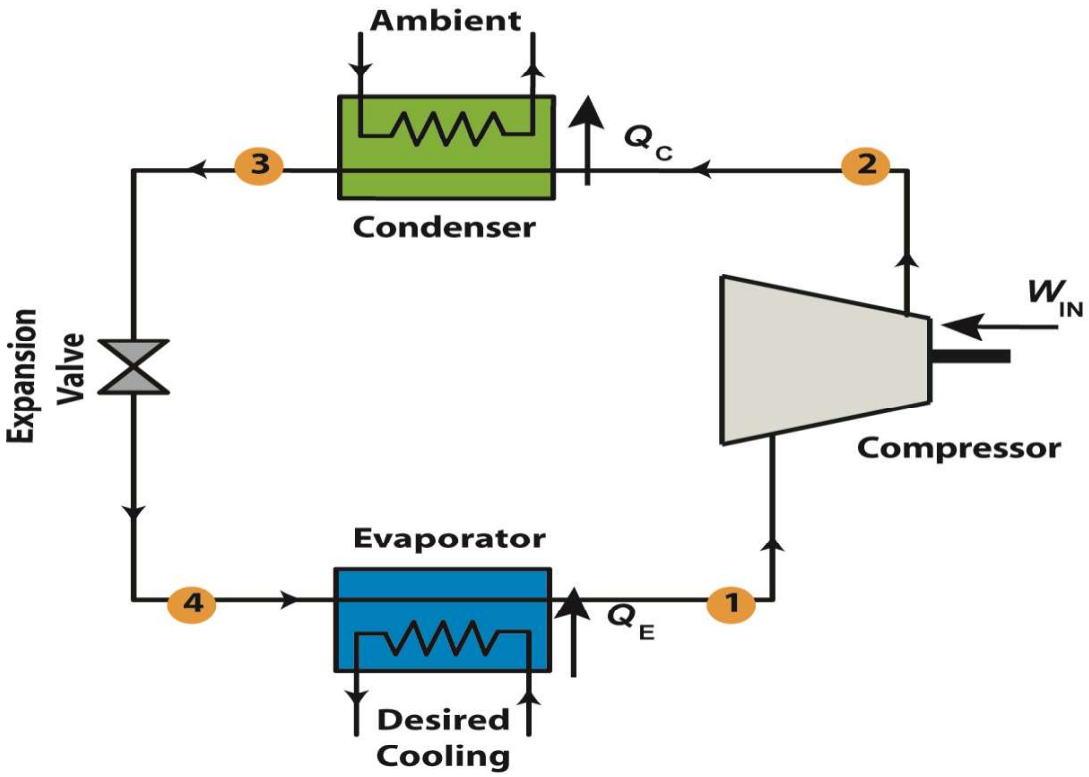

Figure 1. 1 : Vapor compression refrigeration system

Figure 1.2 shows a schematic of a simple lithium bromide-water absorption system. The refrigerant vapor leaves the evaporator at and enters the absorber where the dilute solution (solution with low LiBr concentration) flow is absorbed into the refrigerant (water) as it is cooled, forming a concentrated solution (solution with high LiBr concentration) of refrigerant and absorbent. This absorption of the refrigerant into the absorbent releases a large quantity of heat which must be rejected to the ambient. The concentrated solution is then pumped to the high-pressure side and flows through the solution heat exchanger on

its way to the generator, recuperating some of the heat from the concentrated solution stream, returning to the absorber from the generator. The generator is supplied with heat to separate the refrigerant stream from the solution stream leaving behind a dilute solution stream.

The major difference between an absorption refrigeration system and a traditional vapor compression refrigeration system is that a vapor compression refrigeration system uses a compressor to make the pressure difference required to circulate the refrigerant while the absorption refrigeration system uses a generator chamber and an absorber chamber.

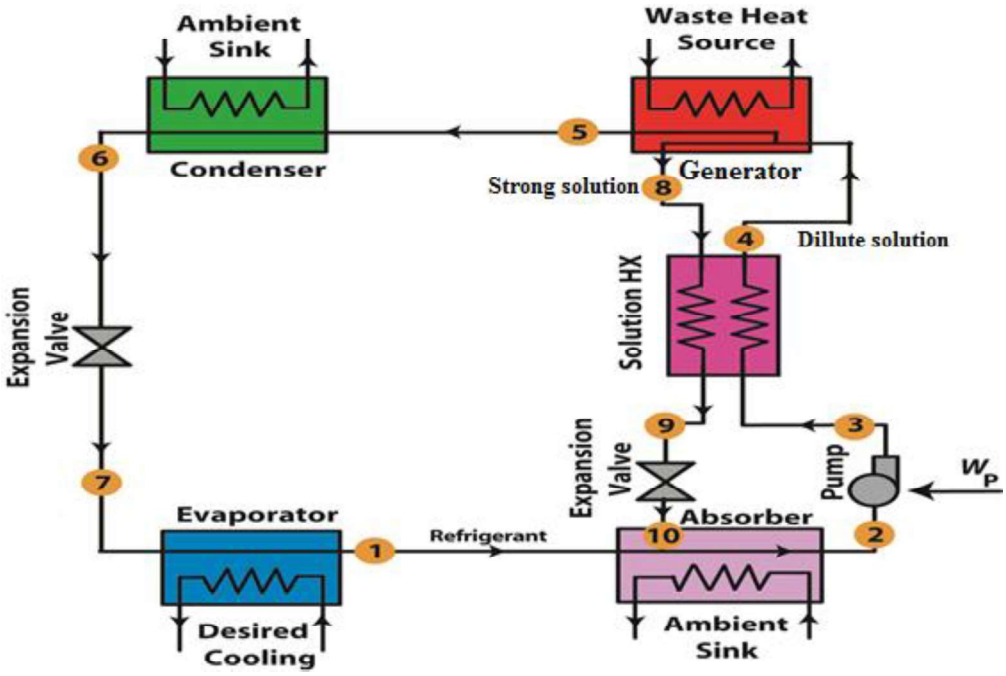

Figure 1. 2 : Single-effect absorption cooling system

1.3 Membrane Distillation (MD) System

Membrane distillation (MD) is one of the separation techniques which is used for water desalination. The membrane systems are generally driven by an external thermal source and use micro-porous hydrophobic membrane material to separate water vapor from feed brackish/salty water [2].

In recent years, MD systems are receiving more interest among researchers because of possibility of operating the membrane module feed/hot side of the at atmospheric pressure. Additionally, due to the studies that mentioned more than 50% of total thermal energies generated worldwide are comprise of the low-grade thermal energies, the MD process can be driven by low-grade thermal energies (e.g. low-temperature heat or waste heat from geothermal or solar systems) [2]. However, in case of remote areas, MD systems can be driven by thermal energy from renewable sources for water production purposes [2].

In operation, the main concept is that only vapor can be transported through the membrane porous wall due to the temperature induced vapor pressure difference and the hydrophobic nature of the membrane which leads to pure water production on the low temperature permeate side by condensing the transferred vapor. The membrane performance is controlled by two factors: the membrane selectivity of the solute in the solution, and the flux of the solvent through the membrane. To gain the best separation results, the membrane must be thermally stable, have high selectivity toward the solutes, have high permeability and high chemical resistance [3].

Membrane separation process is more efficient, faster and cost effective as compared to conventional separation techniques. The membrane separation process has some advantages and disadvantages as listed below [3]:

Advantages:

1. Separation occurs continuously and can be carried under mild conditions.
2. Energy consumption is low.
3. Membrane process can be combined with other separation processes.
4. Separation process can be up-scaled easily.
5. Membranes have different properties and can be adjusted.
6. No pre-treatment is required.

Disadvantages:

1. Membrane fouling, concentration polarization and Low selectivity.
2. Membrane lifetime is short due to fouling and concentration polarization.
3. Membrane systems have not been used for mass production of desalinated water and still are used for small scale applications.

Membrane distillation (MD) system has four different configurations. These configurations differ based on the way of how to condense the produced vapor in the membrane permeate side. Figure 1.3 (a) presents the direct contact membrane distillation (DCMD) system. In DCMD, the membrane material surface in the permeate side is in direct contact with liquid phase. This configuration is quite simple and capable of producing reasonably high flux [4], [5], [6].

Figure 1.3 (b) shows the air gap membrane distillation (AGMD) system. In AGMD, the condensation and membrane surfaces in the permeate side are separated by an air gap. The main advantage of this configuration is its higher energy efficiency [7]. In AGMD, a pure water is required to run in the membrane permeate side. Figure 1.3 (c) presents the sweep gas membrane distillation (SGMD). Sweep Gas Membrane Distillation is a process where the vapor at permeate side can be swept from the hot side using stripping gas and then is condensed in an external condenser. It is used when volatiles are removed from an aqueous solution [8], [9], [10]. In comparison with DCMD and AGMD, SGMD has less heat loss through the membrane and higher mass transfer rates, respectively [9].

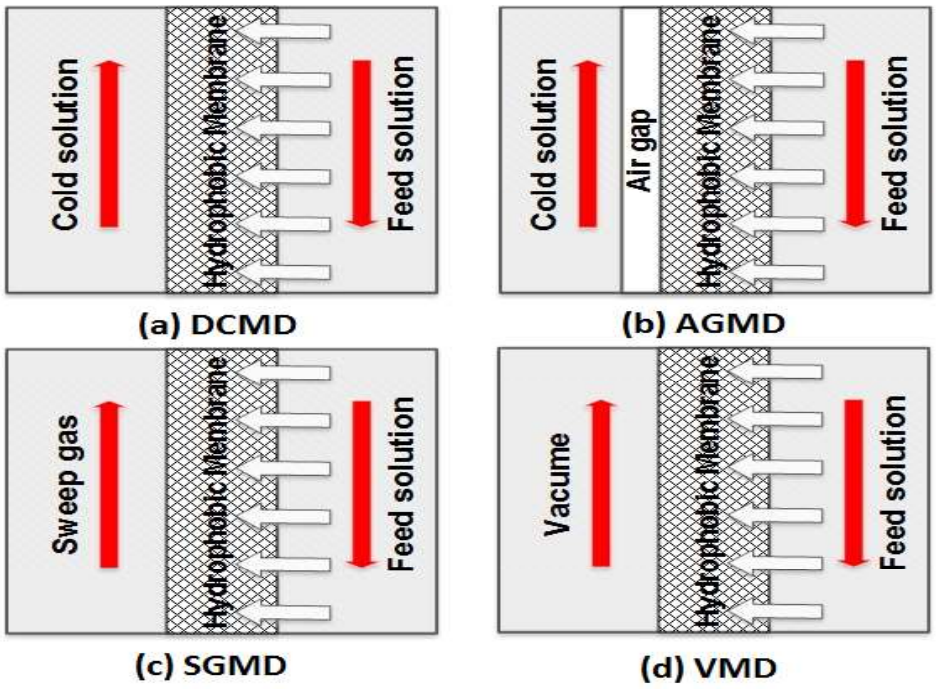

Figure 1. 3 : Membrane distillation system configurations

Figure 1.3 (d) shows the vacuum membrane distillation (VMD) system. Vacuum Membrane Distillation (VMD) is a process in which air (or vapor) under reduced pressure exists in the permeate side, and if needed, permeate is condensed in a separate device. This configuration is useful when volatiles are being removed from an aqueous solution [11], [12].. In VMD, in order to form a vapor pressure difference across the membrane, the vapor permeate is removed continuously from the vacuum chamber.

1.4 Integrated Solar Cooling and Desalination Systems

A number of possible arrangements "paths" from solar energy to various types of thermal desalination systems combined with absorption cooling cycle are shown in Fig. 1.4.

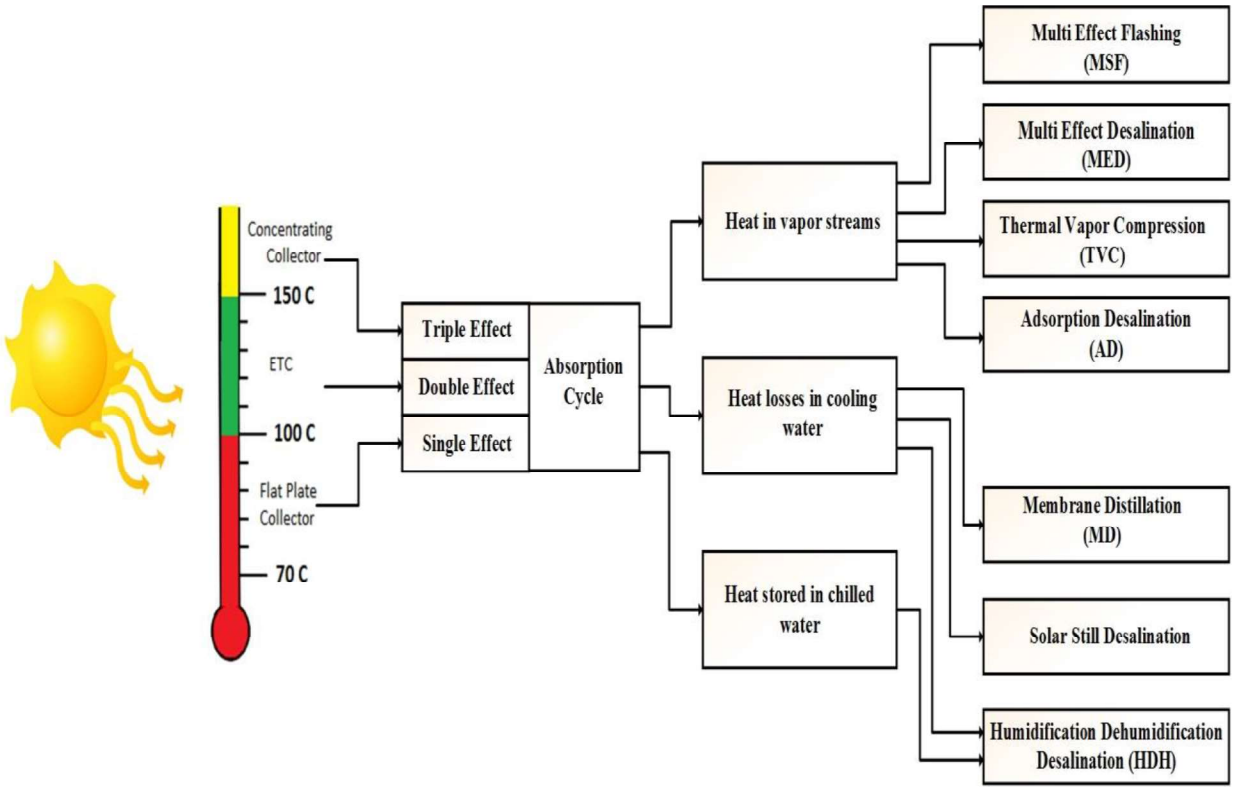

Figure 1. 4 : Integrated Solar Cooling and Desalination system paths

Starting from the inflow of solar energy, there are three types of absorption cycle (single, double and triple effect) according to generation temperature provided by the solar collectors. For solar thermal collectors, different temperature levels are obtained from different collector types. This indicates that the various cycle demands can be matched to temperature level. For instance, the single effect absorption cycle manages at a lower driving temperature whereas the triple effect absorption cycle requires a rather high temperature level of heat supply. Furthermore, there are three significant paths in order to link between solar cooling and desalination systems. These systems can be integrated by replacing the condenser of absorption cycle, make use of the evaporator effect or utilizing the waste heat from the condenser to drive the desalination system.

In the first path, a low temperature MED is assumed to replace the condenser of the absorption cycle, adsorption desalination, low temperature MSF or thermal vapor compression desalination system powered by use of steam that generated in the generator of the absorption cycle. The second path, the waste heat from condenser of the absorption cycle is used heat up the feed water that introduced later to membrane distillation MD, humidification dehumidification desalination HDH or solar still systems. The third path utilize the chilled water coils of absorption cycle evaporator to condense the vapor produced from the desalination system before introduced to the air-conditioning load. Note that, all the previous paths are aimed to co-production of cooling effect and fresh water.

1.5 Motivation

Most of the numerical models carried in the past have developed for single/separate production of chilled as well as fresh water in air conditioning and desalination systems,

whereas few have developed and simulated models that co-generate both of the products. Furthermore, these integrated systems can be driven by use of one of the renewable resources rather than other systems considered in the literature that are mostly driven by fusel fuel or electrical energy. Hence, these technologies are being technical efficient, more economical and environment-friendly. A combined modeling process involves tracking of multiple parameters involved in the cooling and desalination systems because they are inter-linked.

The objective of the present study is to develop an integrated solar absorption cooling and membrane distillation system which is simultaneously produce cooling effect and fresh water, and to analyze the effect of various parameters that affecting the performance including driving temperatures, flow rates and cooling load that govern the performance of the integrated system.

1.6 Research Objectives

The objectives of this work are as follows:

1) Establish a new integrated system that combined solar LiBr-water absorption cooling and direct contact membrane distillation system for simultaneous production of cooling effect and fresh water.

2) Perform a parametric study on the thermodynamic model of the proposed integrated system under different configurations precisely under the most influential parameters that affect the overall system performance.

3) Develop a thermodynamic model for different combined system configurations in order to come up with the best performance.

1.7 Methodology of Proposed Work

The following methodology was adopted for this research work:

- A detailed literature review of combined cooling and desalination systems.
- Development of a steady state thermodynamic model for solar absorption cooling system using EES Software.
- Development of a steady state thermodynamic model for membrane distillation system using EES Software.
- Build a steady state model for the proposed integrated SAC-DCMD system.
- Study the impact of different design and operating parameters of absorption cycle on the performance of the proposed system using Dhahran ambient conditions.

1.8 Thesis Outline

The organization of the thesis is as follows:

- Chapter 1 provides a brief review of the literature on different arrangements and thermodynamic modeling for integrated thermal cooling and desalination systems.
- Chapter 2 outlines overview of LiBr-water absorption cooling cycle, the thermodynamic fundamentals, the individual component models and steady-state modeling of single-effect LiBr-water absorption system.
- Chapter 3 describes various types of membrane distillation systems, the heat and mass model formulation and steady state modeling of DCMD system.
- Chapter 4 presents the arrangement of combined system developed in this study and different configurations for the proposed system.

- Chapter 5 presents overall performance results for the integrated absorption-membrane system responses to different operating conditions and improvements applied in terms of fresh water production.
- Chapter 6 presents the cost analysis conducted for this kind of integrated systems.
- Chapter 7 summarizes the conclusions from the steady state model and provides recommendations for future work.

CHAPTER 2

LITERATURE REVIEW

This chapter presents a review of the thermo-dynamic models and designs implemented for analyzing the performance of solar absorption systems. Moreover, the theoretical and experimental works conducted to improve the productivity of the direct contact membrane systems are outlined. In addition, previous works on the coupling of solar absorption cooling and desalination systems are discussed.

2.1 Solar Absorption Cooling Systems

Among recent cooling systems, a considerable attention has been focus towards solar absorption cooling. The experimental investigation on performance of a continuous, non-storage solar driven absorption refrigeration cycle is performed by Hammad and Audi [13]. The results are presented in terms of variation in the evaporator and generator temperatures. The peak actual coefficient of performance obtained is 0.55. Wang et al. [14], have studied the performance of LiBr–water absorption chiller based on a real developed 50 kW prototype. The results showed that under the range of 95 °C to 120 °C of generation temperature and a group of data of the steady state parameters, the COP increased from 0.69 to 1.08. They also discussed the effect of different design parameter on system performance. They reported that the chiller performance will be higher under low cooling water temperature, high chilled water temperature, high frequency of hot water pump,

optimized HA (high pressure absorber) valve opening and proper frequency of generation pump. Olivier et al. [15], developed a model for single effect, solar operated LiBr-water absorption chiller with 30 kW cooling capacity. The study was conducted for university building in Reunion Island. The results obtained from the developed model showed high reliability in terms of capacities and COP and only 5% differences were reported in term of validation.

Bakhtiari et al. [16], performed an experimental and simulation analysis of 14 kW single-effect LiBr-water absorption system. It was found that over a large range of hot water inlet temperature, the absorption heat pump has almost a constant COP and it is only influenced by the flow rate and cooling stream temperature. The results also indicated that the chilled stream temperature is affected by the cooling capacity rather than generator and cooling stream temperatures. A single-stage combined ammonia-water absorption power and cooling systems that simultaneously produce cooling and mechanical power, powered by different solar thermal technologies have been introduced by Ayou [17]. The proposed model was developed using TRNSYS simulation tool.

Pongtornkulpanich et al. [18], designed and built a 10 ton LiBr-water single-effect absorption cooling system driven by solar energy in Thailand. The study was performed to find the extent to which solar energy replaced conventional energy sources. The results showed that 81% of the yearly average solar fraction can be delivered by solar collectors while a LPG-fired backup heating unit was used to provide the remaining 19% of thermal energy required by the chiller.

A comparative study compared the use of single effect cycles working with H_2O/LiBr and $NH_3/LiNO_3$ as part of the same solar system was carried by Lecuona et al. [19]. The results reported that the $NH_3/LiNO_3$ working couples offer a smaller production above zero Celsius degrees temperatures and does not require higher hot water driving temperatures as compared to H_2O/LiBr. Muye et al. [20], introduced a new arrangement for combined cooling and power cycle driven by low grade solar heat to fulfill the cooling and power needs in buildings in Spain. The results confirmed that the overall annual performance was improved by using the proposed cycle.

2.2 Direct Contact Membrane Distillation Systems

Several attempts have been made in direct contact membrane distillation systems in order to improve water flux produced. However, only specific speculations of the techniques that might improve water flux have been reported in the literature. The theoretical analysis to predict the improvements in the distillate flux of parallel-plate direct contact membrane system were performed by Ho et al. [21]. The improvements are conducted by utilizing roughened surface flow channel for enhancing heat transfer under countercurrent flow operation. The results showed that, with increasing the inlet hot stream temperature and fluid flow rate, the distillate water flux increased. Martineza and Rodriguez [22] have conducted an experiment to measure the effect of including a spacer in the channels of the direct contact membrane module, to enhance the mass transfer characteristics across the membrane which reflects on permeate productivity. They mentioned that, the module and membrane must be adequate in order to achieve a high flux performance.

A comprehensive study on the effect of different parameters on the performance of the DCMD system was presented by Khalifa et al. [23]. They developed an analytical model to predict the system performance of the DCMD system at different operating conditions. The results confirmed that less than 10% deviations from experimental measurements are achieved when the model is used to predict the system performance. Moreover, the results showed that the permeate flux increases with increasing the permeate flow rate, pore size, feed flow rate, feed temperature and decreases with increasing the feed concentration and permeate temperature.

Khayet et al. [24], presented a new approach for the design of novel membranes to be used in DCMD systems. Their design outlined the desired characteristics needed for the membrane such as thickness of the hydrophilic layers and the hydrophobic. Yanbin Yun et al. [25], developed a DCMD model by implementing an experimental setup for high concentration NaCl solution. Their study aimed to measure the permeate flux obtained at different cold and feed temperatures, flow rates and feed concentrations. Furthermore, they proposed a new DCMD model that takes into consideration the effect of membrane fouling and concentration polarization resistances and membrane resistance.

Jiraratananon et al. [26], conducted an experiment to study the heat and mass transfer through direct contact membrane distillation (DCMD) unit that using a flat sheet PVDF membrane with a pore size of 0.22 μm. additionally, they studied the effect of feed temperature and crossflow velocity under the range 40- 70 °C and 1.85-3.7 m/s respectively while fixing the receiving distillate temperature and crossflow velocity 20 °C and 2.92 m/s, respectively. The results showed that increasing the feed temperature and velocity increase the permeate flux obtained while increasing the feed concentration will decreases the flux.

A complete description of transport in a DCMD system as driven by a gradient of vapor pressure is presented by Martinez and Maroto [27]. In their study, several experimental configurations for membrane and module working at different operating conditions have been considered. Runyu Ma et al. [28], have conducted an experiment for DCMD system in which three different pore sizes for three kinds of microporous hydrophobic membranes were employed. They studied three parameter model named the molecular diffusion, Knudsen diffusion and Poiseuille flow transition (KMPT) model in order to predict the permeate flux and the membrane distillation coefficients (MDC) for DCMD.

Martinez and Florido-Diaz [29], have conducted a direct contact membrane distillation experiment based on a dusty- gas model of gas transport through porous media to predict the outcome flux. The results proved that when the permeate and feed are degassed, the permeate flux increased. Moreover, the effect of increasing the recirculation rate is to decrease the temperature polarization, which improves the flux. Lagana et al. [30], presented a model that describes the membrane behavior and fluid dynamics within the direct contact membrane distillation system. They studied the influence of several properties of membrane morphology i.e. pore radius and distribution, thickness and temperature difference through the membrane and other mechanical properties on permeate flux. Simulation results showed that, the pore radius and temperature difference have a minor effect on the flux.

Based on the analysis of mass and heat transfer through the membrane, Lawal and Khalifa [31], studied a theoretical model to predict the performance of Direct Contact Membrane Distillation (DCMD). They subsequently developed a new regression model which focused on analyzing and predicting the effect of four different system operating parameters

(coolant inlet temperature, feed inlet temperature, coolant flow rate and feed flow rate) on performance of DCMD. The results showed that only 1.098%. was recorded as a percentage error between the two models. However, the regression model is more suitable for predicting the performance of DCMD system. Additionally, the feed inlet temperature and coolant inlet temperature showed the maximum overall effects on the permeate flux.

In addition, they presented a model based the concept of heat and mass transfer to evinced the significant effect of membrane coefficient on the permeate flux in DCMD. The developed model was tested on the effect of increasing coolant temperature, feed flow rate and feed temperature. Results revealed that the combined Knudsen-molecular diffusion model was considered the best model for the prediction of permeate flux in DCMD. The results are also showed that as the pore size increases, the permeate flux increases until the pore size reach up to the critical pore condition where there is no change in flux prediction [31].

2.3 Combined Cooling and Desalination Systems

In the last few years, a number of experimental and theoretical studies have been carried out in order to establish the concept of combination between air conditioning and desalination systems. In the field of solar cooling and desalination combination, there are several studies that have been done. Slesarenko [32] presented a thermodynamic analysis described that how the desalination plants can be integrated to heat pumps by use of heat energy effectively. He highlighted that connection of a compression heat pump to a thermal desalination plant will increase by 2-3 times the economical and thermodynamic indicators of the desalination process. Moreover, in term of fresh water production cost, this

connection leads to considerable substantial cost reduction. A comparative simulation and study on the performance of an integrated cooling-desalination system powered by solar energy is presented by Franchini et al. [33]. The combined system composed of 50 kW absorption cooling cycle and humidification dehumidification desalinator. The result reported that an increase in the driving temperature from 90 °C to 110 °C leads to a considerable improvement of fresh water productivity and chiller capacity.

Padilla and Rodriguez [34] demonstrated a new technology based on coupling of a multi-effect distillation unit and a double-effect absorption heat pump. Their study targets to a multi-effect distillation unit that is low-cost, energy efficient and has a zero discharge. They reported that, coupling a multi-effect distillation system to an absorption heat pump could significantly increase the competitiveness of both conventional and solar powered multi-effect distillation plants. Mandani et al. [35] have developed and analyzed a new configuration for combination between the single-effect evaporation and absorption heat pump that utilize liBr water solution. In light of the analysis results, they conclude that the thermal performance ratio varies from 2.4 to 2.8 which is considered 50-70% higher than the conventional single-effect thermal vapor compression and the mass fraction of LiBr in the concentrated solution would not highly affect the system performance.

Yuan et al. [36] have experimentally introduced a model for integrated air conditioning and humidification dehumidification desalination driven by mechanical vapour compression heat pump. The proposed system utilized the cold from evaporator and the heat from condenser of the heat pump sufficiently and partially reuse the latent heat. The results have shown that there is an increase in desalinated water production and the length of humidifier when the flow rate of water and water temperature increase.

Gude and Nagamany [37] developed a model for new low temperature desalination unit combined with modified absorption refrigeration system. In their study, a thermal energy storage system is considered as energy source for low-temperature distillation which utilizes rejected heat by the absorption refrigeration cycle condenser. Both grid power and solar collector system are used to provide the required energy for the generator of the absorption refrigeration system. Based on their simulation results, the combined system was capable of providing 3.25 kW as cooling capacity along with an additional desalinated water of 208 kJ/kg is consumed to produce a rate of 4.5 kg/h as fresh water which obtain a desalination efficiency of 80–90%.

Padilla et al. [38] proposed and validate an experimental design for double-effect absorption heat pump connected to solar desalination system based on multi-effect distillation. The experimental work is conducted in Almeria (Spain) for multi effect desalination unit with nominal performance ratio of 10.5. The validation results have shown that the overall performance ratio is 20, which leads to significant reduction in the solar field area required by 50% compared to individual solar multi effect desalination system.

Wang and Lior [39], [40] proposed a mathematical model for high efficiency combined water desalination unit and refrigeration system using LiBr-H_2O absorption cycle. The results showed that 42% energy saving rate is achieved, compared to individual water-only and refrigeration-only systems. The coefficient of performance of the absorption refrigeration heat pump is around 1.6. They are also mentioned that using steam of higher pressure as driving heat source will increase the multiple effect evaporation unit effects and thus more fresh water will be produced. In their later study, they performed an

economic and thermal performance analysis for integrated low temperature multi effect evaporation water desalination and LiBr absorption heat pump system. In the light of the results, as the generator of the absorption heat pump reached high temperatures, the energy utilization by combined system is improved. The pressure of the heating steam for multi effect evaporation unit is increased using a high pressure driving steam which consequently increase the number of effects of the desalination unit and thus increasing the desalination yield for the same energy input.

Ghali et al. [41] theoretically and experimentally studied the optimization of a combined solar still unit and air conditioning system to meet the fresh water and specific cooling load needs for a residential application. The optimization analysis of the combined air conditioning and solar distiller system operation have been conducted for a residential case of study which has a 5.4 kW cooling load and a daily fresh water demand of 100 liters over 10 hours of integrated system operation. The simulation results showed that the total energy consumption for optimal operation is varied between 21.34 to 23.80 kWh/day.

The combination between solar still desalination and vapor compression refrigeration system has been experimentally studied by Abdel-Rehim and Lashine [42]. Their work is aimed to obtain the daily fresh water production from the solar still while meeting the hourly air conditioning load for the space application, so the system is tested for day and night times of operation for the summer month June. The operation of the proposed system is to utilize the heat sink of the evaporator and the released heat from the condenser of the air conditioning system. The experimental results showed that the maximum fresh water productivity through June is 37 liters in night-time of June 3 and 29 Liters in daytime of

June 5. They mentioned that the average cost of one liter of fresh water produced from the combined system is 0.021441 (LE).

Abdulrahim and Darwish [43], proposed a new arrangement of a combined low temperature, multi-effect distillation and H_2O-LiBr absorption refrigeration system as illustrated in Fig. 2.1. In their work, an absorption cycle has been used to supply high pressure, high temperature saturated steam as heat source in the first stage of the desalination system as well as providing chilled water for thermal comfort purposes considering the solar irradiance as a driving source for the cycle. The simulation results showed that the cooling load can influence the amount of distillate water produced but maintains the gain output ratio at constant value. Furthermore, as the cooling capacity increased, the heat transfer fluid flow rate and the solar field area required were increased.

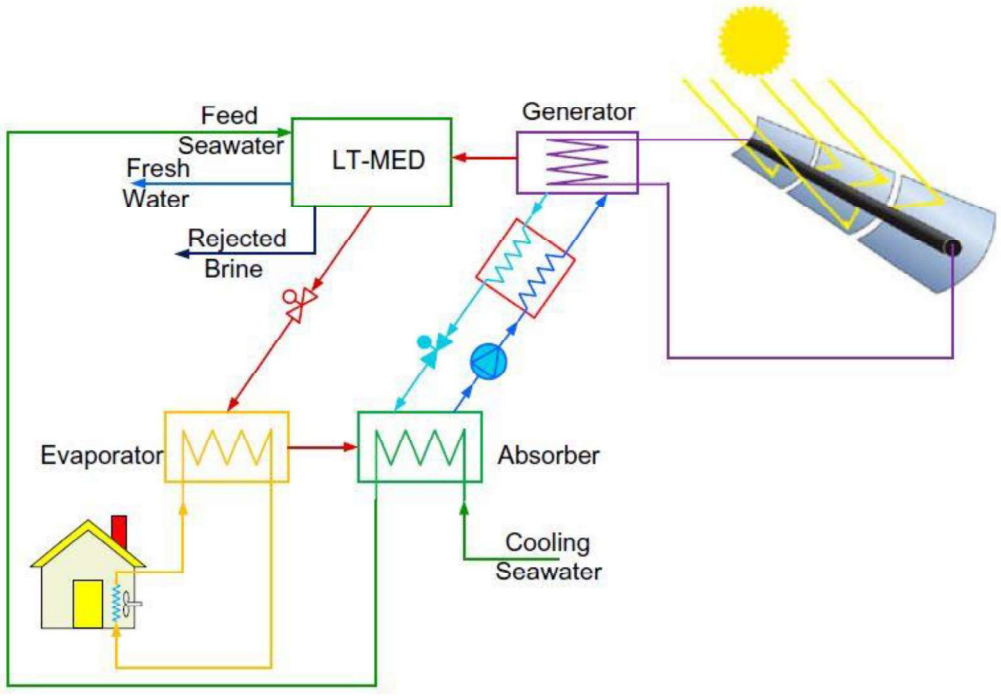

Figure 2. 1 : Configuration for integrated absorption cooling and MED desalination [43]

Chiranjeevi and Srinivas [44] have modelled and simulated a two stage humidification dehumidification desalination system combined with solar thermal cooling system as shown in Fig. 2.2. In their work, a flat plate collector has been selected for HDH desalination unit and a concentrating collector for single effect vapor absorption refrigeration system. The results indicate that with the proposed integration, the distillate yield is increased per one stage humidification dehumidification system. They concluded that the resulted cooling capacity and distilled water of the integrated system are 75 kW at volume of air and 670 liters per hour, respectively. In their later study, they conduct a simulation study for the proposed system and the recorded readings are experimentally validated on the pilot plat. The main sequence of the proposed system is that the saline water is heated in a separate solar water heater and supplied to two air heaters and humidifiers.

They mentioned that the simulation results are extremely matched with the experimental results generated from the plant. The obtained fresh water is 100 mL per $m^3$of air. Approximately 150-200W of cooling capacity is resulted at the exit of the desalination unit. The benefits of the second stage desalination are experimentally proved for the purpose of increasing the desalinated water production and cooling effect. Nada et al. [45] have carried out an experimental study to investigate a hybrid air conditioning system using vapour compression refrigeration cycle and humidification dehumidification water desalination.

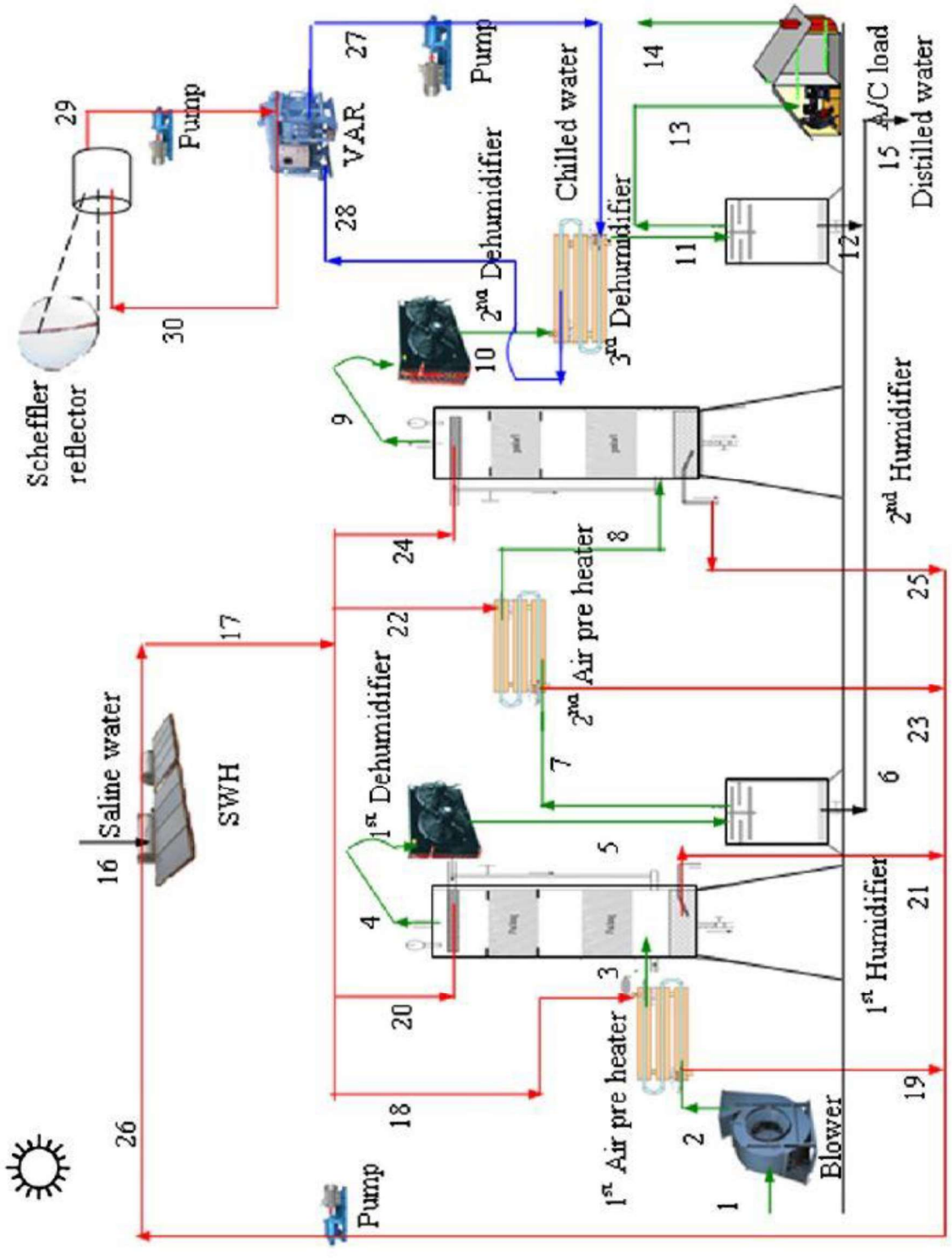

Figure 2. 2 : Configuration for integrated absorption cooling cycle and HDH system [44]

The study has focused on analyzing the effect of four different system operating parameters on desalinated water production rate. The results obtained from their experimental work have shown that the refrigeration capacity, the compressor work, and the rate of fresh water production per kilogram of fresh water are enhanced as the specific humidity and mass flow rate for the air are increased.

The integration between air-conditioning and humidification dehumidification desalination systems is proposed by Nada et al. [46]. The theoretical investigation has been carried out for the performance of the systems which used for the purpose of energy saving and fresh water production at the same time. The results indicated that there is an increase in the powers saving and fresh water production rates of the proposed systems when the supply air temperature and fresh air ratio are increased. As the wet bulb temperature of outdoor increase, the rates of fresh water production and powers saving are increased and decreased respectively. They are also mentioned that the water production rate is increased remarkably when the evaporative cooling located after the fresh air mixing.

Fathalah and Aly [47] is presented a theoretical study for a solar powered combined system comprising a multi effect desalination unit (MED) and a LiBr-H20 absorption cooling machine. The MED unit is powered by the waste heat of the absorption machine while the overall system is powered by medium parabolic concentrators. The results revealed that, for a given cooling load of 100 ton refrigeration, the system can produce up to 40 m3 of fresh water. The overall COP reaches 1.44 which is more than twice that of a conventional absorption machine at the same temperature levels.

The following conclusions can be made based on the literature review:

1. Thermal absorption cooling systems are the most suitable option to be powered by solar energy compared to solar photovoltaic-vapor compression cooling systems.
2. LiBr-water absorption system presents so far best proven absorbent-refrigerant working pair for cooling applications.
3. Direct contact membrane distillation system is shown to be quite simple in design and it is capability to produce reasonable high flux.
4. Integrating solar cooling cycles with desalination systems will improve the overall system efficiency as well as achieves environmental benefits.

A summary for previous studies in combined AC-MD system is shown in Table 2.1. However, none of the researchers studied in the preceding survey studied the combination between solar-powered LiBr-H_2O absorption cycle and direct contact membrane distillation unit for simultaneous supply (co-production) of fresh water as well as cooling effect as illustrated in review summary. Hence, in the present research, a new design and analysis for an integrated solar-powered absorption LiBr-H_2O and direct contact membrane distillation system are discussed in detail.

Table 2. 1 : Literature review summary for integrated AC-Desalination systems

Reference	Cooling System	Desalination System	Combined System Capacity	Heat source	Notes
Fathalah & Aly (1991) [47] (Theoretical)	Absorption Refrigeration system	Multi Effect Desalination (MED)	100 TR – 40 m^3/day	Solar Energy	(1) The overall coefficient of performance (COP) was 1.44, which is more than double that for the absorption machine alone over the same temperature range.
Mandani et. al. (2000) [35] (Theoretical)	Absorption Refrigeration system	Single Effect Evaporation (SEE)	N/A	Heating steam	(1) Thermal performance ratio was closed to 50-70% higher compared to conventional single-effect thermal vapor compression. (2) The mass fraction of LiBr in strong solution has no significant effect on the system performance.
Yuan et. al. (2005) [36] (Experimental)	Mechanical Vapor Compression Chiller	Humidification Dehumidification Desalination (HDH)	500 W – 2.5 kg/h	Electrical power	(1) The fresh water productivity increased with the water flow rate, water temperature and the humidifier length. (2) The overall efficiency increased to 3.6 compared to 3.0 (COP) for separate air conditioning system.
Giuseppe et. al. (2007) [33] (Theoretical)	Absorption Refrigeration Chiller	Humidification Dehumidification Desalination (HDH)	50 kW – (varied)	Solar Energy	(1) They introduced the variation of overall system performance with respect of heat source temperature. (2) The increase of the heat source temperature from 90°C up to 110°C leads to an improvement in chiller capacity and fresh water productivity: nevertheless, the overall efficiency was higher only for high sea water temperatures and low coolant flow rates.

Reference	Cooling System	Desalination System	Combined System Capacity	Heat source	Notes
Nagamany & Gude (2008) [37] (Theoretical)	Absorption Refrigeration system	Desalination unit includes (two heat exchangers, an evaporation chamber, three columns and condenser).	3.25 kW – 4.5 kg/h	Grid power & Solar Energy	(1) The system requires thermal energy storage volume of 10 m3 can achieve a desalination efficiency of 80–90%. (2) The proposed system has low energy requirements compared to a separate multi-stage flash desalination.
Abdel-Rehim & Lashine (2009) [42] (Experimental)	Mechanical Vapor Compression Chiller	Solar Desalination Still	2.5 hp (1.86 kW) - 37 L/day	Electrical power	(1) The maximum efficiency recorded for the proposed system was 40% compared to 25% for conventional solar still. (2) The average cost of one liter of distillate water from the combined system = 0.021441 (LE).
Rodriguez et. al. (2010) [38] (Experimental)	Double Effect Absorption Refrigeration system	Multi Effect Desalination (MED)	150 kW – 2.7 m^3/h	Solar Energy	(1) The overall performance ratio was 20. (2) The required solar field area was 50% lower than that required for separate solar MED system.
Wang & Lior (2011) [40] (Theoretical)	Absorption Refrigeration system	Multi Effect Desalination (MED)	1652 kW – 4 kg/s	Motive Steam	(1) The number of effects of the MEE unit increased with higher pressure of driving steam which results in an increase in fresh water productivity. (2) 42% was achieved as energy saving rate compared to individual water-only and refrigeration-only systems.

Reference	Cooling System	Desalination System	Combined System Capacity	Heat source	Notes
Ghaddar et. al. (2011) [41] (Theoretical)	Mechanical Vapor Compression Chiller	Conventional Solar Still	5.4 kW – 100 L/day	Electrical power	(1) The excess electrical energy cost to maintain the desired need of fresh water was 0.11 kWh/liter.
Chiranjeevi & Srinivas (2014) [44] (Theoretical)	Single Effect Absorption Refrigeration system	Two Stage Humidification Dehumidification Desalination (HDH)	75 kW (20 TR) – 670 L/h	Solar energy	(1) They introduced the concept of cooling effect sharing between the cooling load (5TR) and desalination unit (15 TR). (2) The final energy utilization factor (EUF) for the cycle and plant were 0.58 and 0.33, respectively.
Abdulrahim & Darwish (2014) [48] (Theoretical)	Absorption Refrigeration	Low Temperature Multi Effect Desalination (MED)	1500 kW – 3.72 kg/s	Solar energy	(1) They studied the effect of the cooling load on the performance of the combined system. (2) Increasing the cooling load increased the distillate water, required solar field area and the flow rate of the heat transfer fluid but keeps the GR constant at 5.7.
Nada et. al. (2015) [45] (Theoretical)	Mechanical Vapor Compression Chiller	Humidification Dehumidification Desalination (HDH)	1000 TR – 86 Tone/day	Electrical power	(1) The fresh water production rate increased with increasing fresh air ratio, supply air temperature and outdoor wet bulb temperature. (2) Power saving and the total cost saving increased with increasing fresh air ratio, supply air temperature and decreasing outdoor wet bulb temperature.

CHAPTER 3

SOLAR ABSORPTION

REFRIGERATION SYSTEM

This chapter provides the necessary background on the working principles of LiBr-water absorption cycle. A brief introduction to steady-state modeling of the heat exchangers are summarized. The thermodynamic fundamentals summarized in this chapter form the basis for the development of the integrated solar absorption and desalination model (Chapter 5).

3.1 System Overview

The proposed single effect lithium bromide-water absorption cycle comprises of a generator, an absorber, condenser, evaporator, solution and refrigerant expansion valves, solution heat exchanger and solution pump. A schematic describes the working principle of the single-effect lithium bromide-water absorption cycle is shown in Fig. 3.1. Numbers on the connecting lines represent assigned state points.

In the generator, a relatively high temperature heating fluid heated in a solar collector flows into tubes immersed in a dilute LiBr-water solution (11-12). A relatively weak LiBr-water solution (3) leaving the absorber through a solution heat exchanger enters the generator.

After heat exchange with hot water (11) inside the generator (Q_g), the solution absorbs heat from the hot water causing the refrigerant (water) to boil off (vaporize) under high pressure and separate from the solution. After separation, the refrigerant (water vapor) produced (7) leaves the solution through evaporation. The solution becomes more concentrated and exits the generator. Hot fluid stream (12) flows back to the solar collector to reheat again utilizing the solar irradiance. The refrigerant (7) leaving the generator is assumed to be pure water vapor and doesn't carry any amount of water content because it will affect the capacity of the refrigeration system. High-pressure, high temperature water refrigerant (7) in the vapor state flows into the condenser. Inside the condenser, the water vapor (7) undergoes condensation by rejecting the heat (Q_c) to cooling sea-water (15) and exits as a liquid refrigerant (8).

The condensed water refrigerant (8) formed in the condenser enters a throttling valve where it expands. Then, the low pressure and high pressure sides of the cycle is separated due to a liquid seal created by the throttling valve. The pressure of water refrigerant drops to that of the evaporator while it flows through the expansion device. During the throttling process, the temperature is reduced even more so that the required refrigeration effect can be obtained at the required evaporator temperature and pressure. Inside the evaporator, heat from the conditioned space (Q_e), is removed to produce the desired cooling effect. The throttled refrigerant (9) is sprayed over the evaporator's tube bundle that acts as heat exchanger. The evaporation of the throttled water refrigerant inside the evaporator takes place by taking in the heat of condensation from a connected cooling water that needs to be chilled (17).

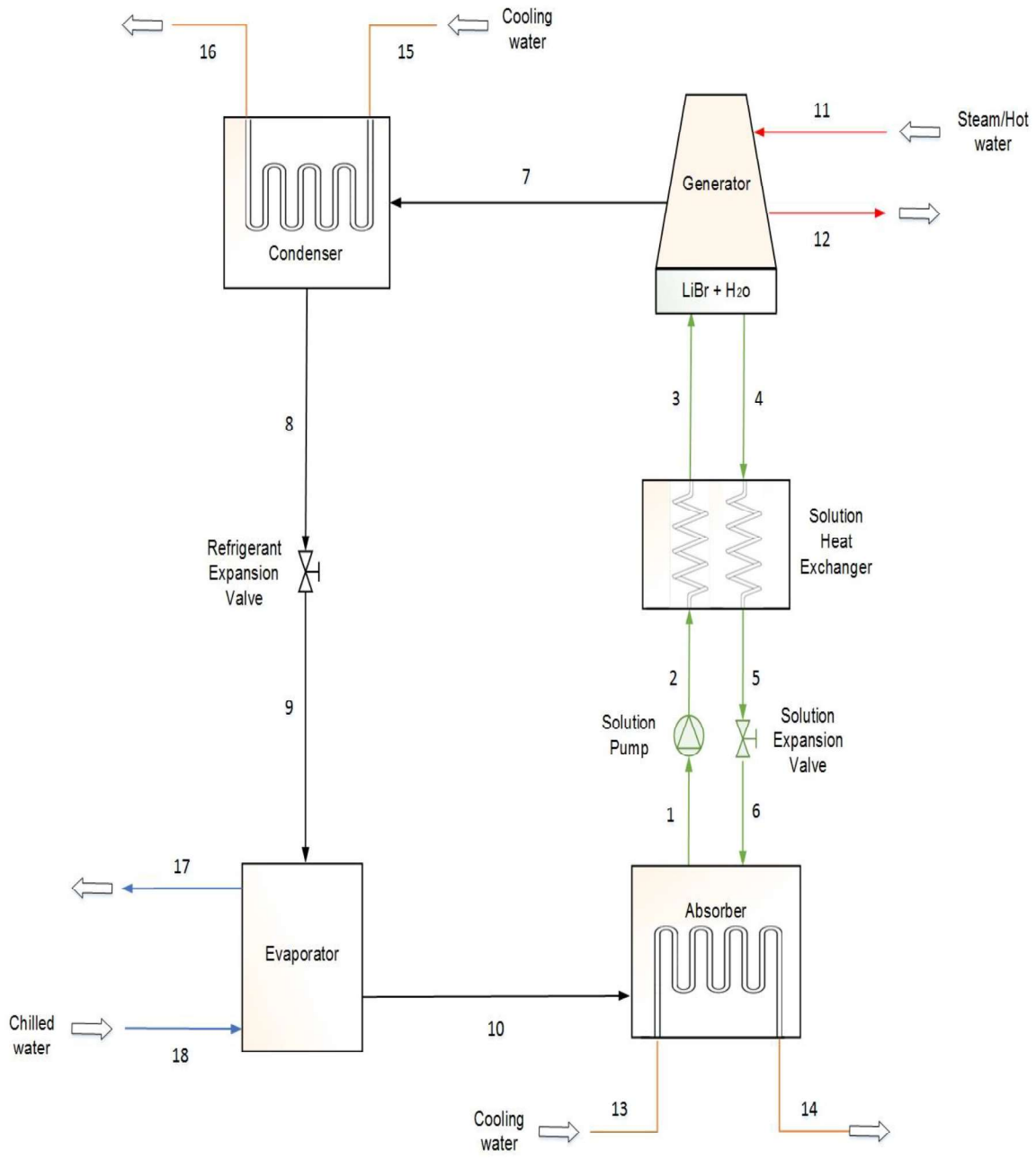

Figure 3. 1 : Proposed absorption refrigeration system

The saturated water vapor (10) from the evaporator then flows into the absorber. The enriched solution (4), (where the concentration of LiBr in water is high), that leaves the generator passes through solution heat exchanger and throttling valve represented by (5 and 6), respectively. Then the strong solution sprayed into the absorber. The absorption

of superheated low pressure water vapor (10) takes place inside the absorber when it comes in contact with the low temperature, strong LiBr-water solution (6) coming from solution heat exchanger, then the strong solution (6) becomes a dilute solution (1). The absorption of water vapor in strong solution lowers the pressure in the absorber which in turns draws more water vapor from the evaporator and thus raise the temperature of solution.

The absorber's tubes which has a cooling water (13) flowing inside removes the latent heat released during the absorption process ($\mathbf{Q_a}$). Following the absorption process, the dilute LiBr-water (1) is pumped using a solution pump back to the LiBr-water generator through the solution heat exchanger to complete the cycle. However, this solution pump increases the pressure of the weak solution and consumes small amount of external work to operate. The solution heat exchanger reduces the temperature of the strong LiBr-water by transferring heat to the weak LiBr-water solution.

3.2 Thermodynamic Analysis

The steady-state modeling procedure for each internal component of solar absorption refrigeration cycle is discussed in this section.

3.2.1 Generator

Figure 3.2 represents the control volume of the generator. Heat transfer between the coupling fluid and solution is used to separate the refrigerant vapor from the solution. The refrigerant vapor moves towards the condenser and the enriched solution exits the bottom of the generator and enters the solution heat exchanger.

The mass and species balances are carried out inside the generator.

$$\dot{m}_{ws} = \dot{m}_{ss} + \dot{m}_r \tag{3.1}$$

$$\dot{m}_{ws} * X_{ws} = \dot{m}_{ss} * X_{ss} + \dot{m}_r * X_r \tag{3.2}$$

Where X_r, X_{ws} and X_{ss} are the concentration for the refrigerant, weak liBr-water solution and strong liBr-water solution, respectively.

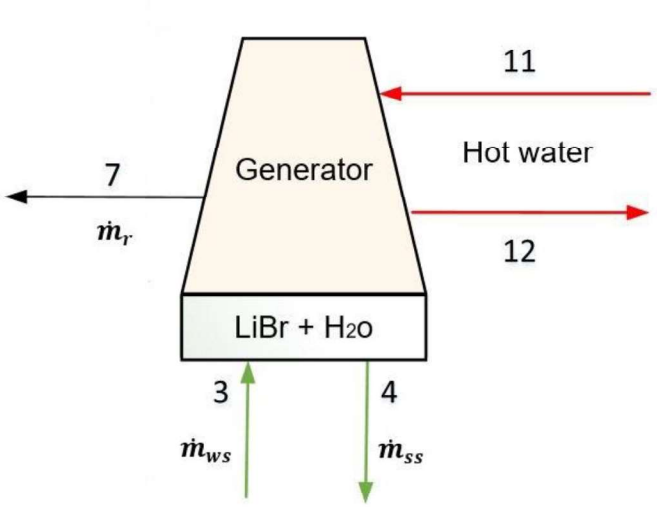

Figure 3. 2 : Generator control volume

From Eqs. (3) and (4), the flow rates of the strong and weak solutions can be determined:

$$\dot{m}_{ws} = \frac{X_{ss}}{X_{ss} - X_{ws}} \dot{m}_r \tag{3.3}$$

$$\dot{m}_{ss} = \frac{X_{ws}}{X_{ss} - X_{ws}} \dot{m}_r \tag{3.4}$$

The overall energy balance on the solution side of the generator is shown in Equation (3.5).

$$\dot{Q}_g = \dot{m}_{ss} * h_4 + \dot{m}_r * h_7 - \dot{m}_{ws} * h_3 \tag{3.5}$$

The corresponding heat transfer rate for the coupling fluid side of the generator is given by:

$$\dot{Q}_g = \dot{m}_{11}(h_{11} - h_{12}) \tag{3.6}$$

3.2.2 Condenser

Figure 3.3 represents a control volume for the condenser. The refrigerant at vapor state that leaves the generator flows into the condenser and enters on the refrigerant side, while cooling water enters the condenser on the coupling fluid side.

The mass and species balances are carried out inside the condenser.

$$\dot{m}_7 = \dot{m}_8 = \dot{m}_r \tag{3.7}$$

The heat transfer rate of the condenser for the refrigerant side of is shown in Equation (3.8).

$$\dot{Q}_c = \dot{m}_r(h_7 - h_8) \tag{3.8}$$

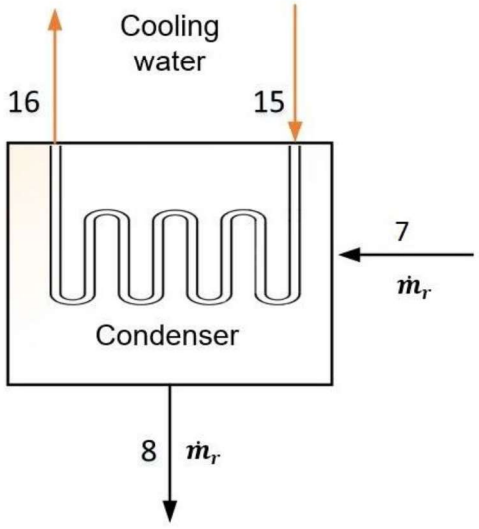

Figure 3. 3 : Condenser control volume

The corresponding heat transfer rate on the coupling fluid side is given by:

$$\dot{Q}_c = \dot{m}_{15}(h_{16} - h_{15}) = U_c\, A_c\, LMTD_c \tag{3.9}$$

3.2.3 Refrigerant Expansion Valve

The solution and refrigerant expansion valves are assumed to be isenthalpic and are represented by Equations (3.10) to (3.13), respectively.

$$\dot{m}_5 = \dot{m}_6 = \dot{m}_{ss} \tag{3.10}$$

$$h_5 = h_6 \tag{3.11}$$

$$\dot{m}_8 = \dot{m}_9 = \dot{m}_r \tag{3.12}$$

$$h_8 = h_9 \tag{3.13}$$

3.2.4 Evaporator

Figure 3.4 shows the control volume for the evaporator. The refrigerant from the expansion valve flows on the refrigerant-side and the coupling fluid flows on the other side. the refrigerant evaporates due to heat supplied by the coupling fluid entering at a temperature 25 °C.

The mass and species balances are carried out inside the evaporator.

$$\dot{m}_9 = \dot{m}_{10} = \dot{m}_r \tag{3.14}$$

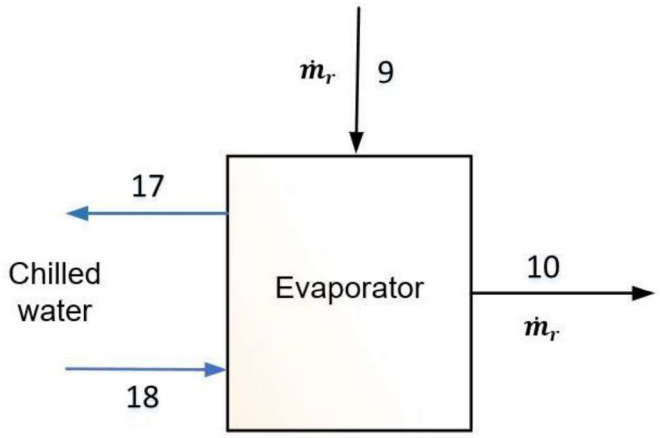

Figure 3. 4 : Evaporator control volume

The heat transfer rate of the evaporator for the refrigerant side is estimated using Equation (3.15).

$$\dot{Q}_e = \dot{m}_r(h_{10} - h_9) \tag{3.15}$$

The corresponding heat transfer rate for the chilled water side is given by:

$$\dot{Q}_e = \dot{m}_{17}(h_{17} - h_{18}) \tag{3.16}$$

3.2.5 Solution Heat Exchanger

Figure 3.5 represents the control volume of the solution heat exchanger. Heat rejected by the concentrated solution flowing on one side is used to heat the dilute solution flowing on the other side. The heat transfer rate between the dilute solution and returning concentrated solution flowing toward the generator is calculated for the two sides of the solution heat exchanger as follows:

$$\dot{Q}_{SHE_1} = \dot{m}_{ss}(h_4 - h_5) \tag{3.17}$$

$$\dot{Q}_{SHE_2} = \dot{m}_{ws}(h_3 - h_2) \tag{3.18}$$

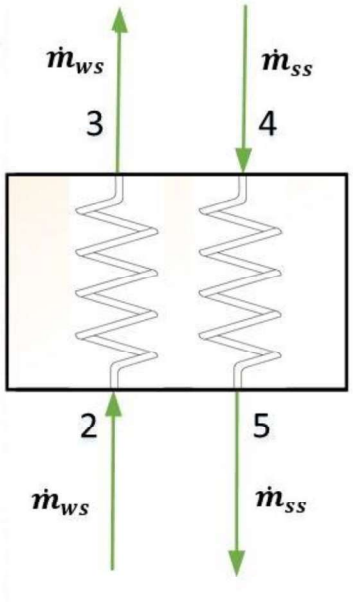

Figure 3. 5 : Solution heat exchanger control volume

3.2.6 Solution Pump

The solution pump is assumed to be isenthalpic and is represented by Equation (3.19).

$$\dot{m}_1 = \dot{m}_2 = \dot{m}_{ws} \tag{3.19}$$

The pumping work through the solution pump can be representing as:

$$W = \frac{v_1 * (P_{high} - P_{low})}{\eta_p} \tag{3.20}$$

The heat transfer rate of the solution pump is estimated using Equation (3.21).

$$\dot{W}_p = \dot{m}_{ws}(h_2 - h_1) \tag{3.21}$$

3.2.7 Absorber

Figure 3.6 represents the control volume for the absorber. The refrigerant vapor exits the evaporator, and the concentrated solution from the solution expansion valve enter the absorber at one end, and mix adiabatically.

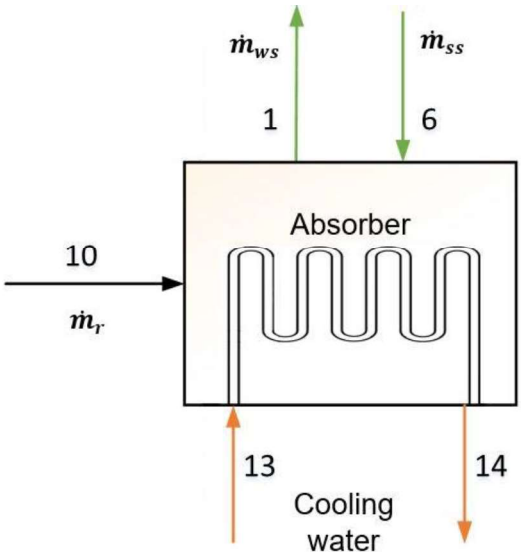

Figure 3. 6 : Absorber control volume

The mass and species balances are carried out inside the absorber.

$$\dot{m}_{ws} = \dot{m}_{ss} + \dot{m}_r \tag{3.22}$$

$$\dot{m}_{ws} * X_1 = \dot{m}_r * X_{10} + \dot{m}_{ss} * X_6 \tag{3.23}$$

The absorber heat transfer rate is estimated as follows:

$$\dot{Q}_a = \dot{m}_{ss} * h_6 + \dot{m}_r * h_{10} - \dot{m}_r * h_1 \tag{3.24}$$

The corresponding heat transfer rate on the coupling fluid side is given by:

$$\dot{Q}_a = \dot{m}_{13}(h_{14} - h_{13}) \tag{3.25}$$

3.2.8 Coefficient of Performance

The cooling mode COP of the absorption heat pump is calculated as:

$$COP = \frac{\dot{Q}_e}{\dot{Q}_g + \dot{W}_p} \tag{3.26}$$

3.3 Results and Discussion

3.3.1 Steady State Modeling

To simplify the formulation and consequent implementation of the model, the following assumptions are made:

1. Steady-state operation.

2. The refrigerant flows through the evaporator and condenser is assumed to be pure water vapor.

3. Saturated liquid state is assumed for refrigerant exiting the condenser.

4. Saturated vapor state is assumed for refrigerant exiting the evaporator.

5. The efficiency of the solution pump is 75%.

The cooling load has been estimated to fulfill the cooling requirements of a typical family living house in Dhahran, Saudi Arabia. A 11 kW has been considered as hourly average value for the cooling load [49]. A numerous simulations are done by using EES to assess the performance of the system. The program is based on heat and mass balances, heat transfer equations and the state equations for the thermodynamic properties of lithium bromide–water. The state equations were evaluated by the thermodynamic properties of LiBr and water available in the library of EES [50].

The initial conditions used by the program include the heat exchanger effectiveness, cooling load and external loops inlet temperature and mass flow rate. The design and operation conditions of the absorption cooling cycle are shown in Table 3.1. With the given parameters, the program calculates at all points of the cycle the values of temperature, enthalpy, pressure, mass flow rate and concentrations for the steady state reached as shown in Tables 3.2 and 3.3.

Table 3. 1 : Baseline inputs defining absorption system operating conditions

Input Name	Value
Cooling capacity (Q_e), kW	11
Absorber temperature (T_a), °C	35
Condenser temperature (T_c), °C	35
Generator temperature (T_g), °C	86
Evaporator temperature (T_e), °C	2
Solution heat exchanger effectiveness ($\in_{shx}$)	0.7
Generator inlet from heating source (T_{11}), °C	93
Generator outlet to heating source (T_{12}), °C	88
Absorber cooling water inlet temperature (T_{13}), °C	25
Absorber cooling water outlet temperature (T_{14}), °C	33
Condenser cooling water inlet temperature (T_{15}), °C	25
Condenser cooling water outlet temperature (T_{16}), °C	38
Evaporator inlet chilled water temperature (T_{17}), °C	10
Evaporator outlet chilled water temperature (T_{18}), °C	5

Table 3. 2 : Energy flows at the various components of the system

Description	Symbol	Energy flow
Evaporator	Q_e	11.00
Absorber	Q_a	14.03
Generator	Q_g	14.76
Condenser	Q_c	11.74
Coefficient of performance	COP	0.746

Table 3. 3 : Absorption system simulation results

Reference point	T (°C)	h (kJ/kg)	m (kg/s)	p (kPa)	LiBr (%)
1. Absorber outlet	35.0	93.4	0.0502	0.706	57.5
2. Pump outlet	35.0	93.4	0.0502	5.627	57.5
3. Generator inlet from SHX	64.7	152.8	0.0502	5.627	57.5
4. Generator outlet	86.0	219.9	0.0455	5.627	63.4
5. Absorber inlet from SHX	50.3	154.4	0.0455	5.627	63.4
6. Solution inlet in absorber	47.0	154.4	0.0455	0.706	63.4
7. Condenser inlet	86.0	2660	0.0047	5.627	0.0
8. Condenser outlet to expansion valve	35.0	146.6	0.0047	5.627	0.0
9. Evaporator inlet from expansion valve	2.0	146.6	0.0047	0.706	0.0
10. Vapor from evaporator to absorber	2.0	2504	0.0047	0.706	0.0
11. Generator inlet from heating source	93.0	389.6	0.7014		
12. Generator outlet to heating source	88.0	368.5	0.7014		
13. Absorber cooling water inlet	25.0	104.8	0.4190		
14. Absorber cooling water outlet	33.0	138.2	0.4190		
15. Condenser cooling water inlet	25.0	104.8	0.2157		
16. Condenser cooling water inlet	38.0	159.1	0.2157		
17. Evaporator inlet from conditioned building	10.0	42.0	0.5246		
18. Evaporator outlet to conditioned building	5.0	21.0	0.5246		

To find suitable conditions when the cycle is driven by solar energy, a sensitivity analysis was performed for the generator, that is, all the conditions (flow rates, heat coefficients, etc.) used in the simulations are maintained constant except for the generator inlet temperature (heat source temperature). The generator provides sensible heat and latent heat of vaporization. The sensible heat raises the inlet solution temperature to the saturation temperature. The latent heat consists of the heat of vaporization of pure water and the latent heat of mixing of the liquid solution. Therefore, the effect of heat source temperature on the absorption system components heat transfer rates, mass flow rates and system efficiency are studied over a range of temperatures from 80 °C to 120 °C, and all the results are shown in Figs. 3-7 to 9.

The effect of heat source temperature on the COP of the absorption cycle are presented in Fig. 3.7. It can be noticed that with variation in the heat source temperature from 80 to 90 °C results in a significant increase in the COP from 0.15 to 0.75. Then followed by a slower rate up to 0.76 to take almost a constant value thereafter. The COP is relatively sensitive to changes in the heat source temperature from 80 to 90 °C. Therefore, this requires that in phase of design and development of the solar collector, it is necessary to look for the constructive option that guarantees temperature of the heat source within the range of 80 to 100 °C.

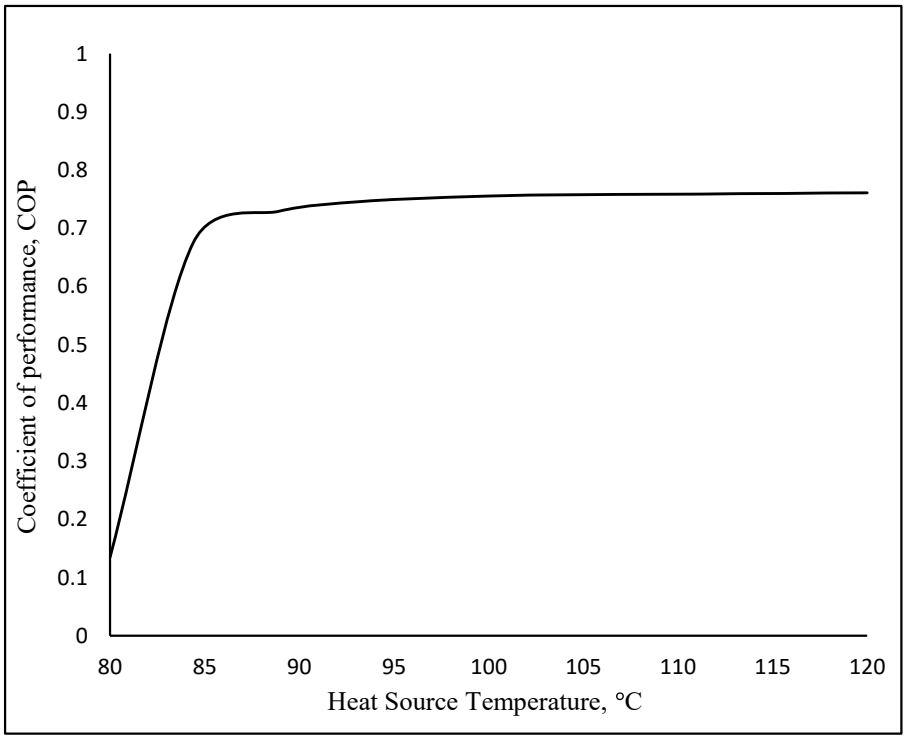

Figure 3. 7 : Effect of heat source temperature on system capacity and COP

The variation in the heat transfer rates on each component of the absorption system with the heat source temperature is illustrated in Fig. 3.8. As expected, the heat transfer rate in each heat exchanger is increased with the increase in heat source temperature. This due to the increase in the solar heat gain which introduced to the generator which results in an increase in refrigerant vapor produced and cooling capacity and accordingly increases the heat transfer rate in the condenser, absorber as well as evaporator.

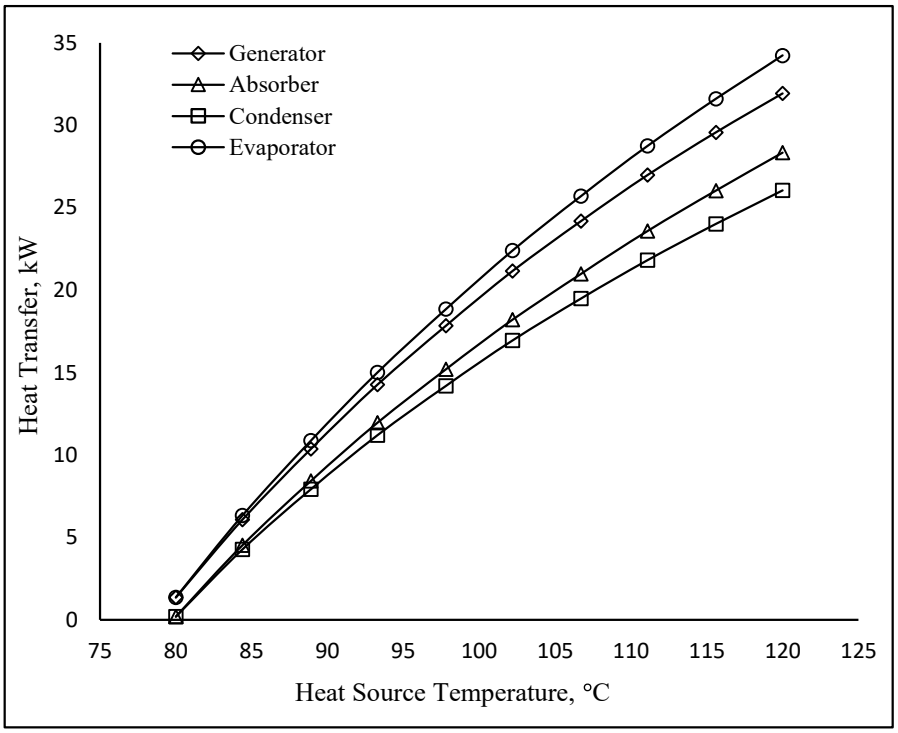

Figure 3. 8 : Effect of heat source temperature on heat transfer of absorption cycle components

The effect of heat source temperature on condenser cooling water, heating fluid and the chilled water mass flow rates are presented in Fig. 3.9. As the heat source temperature of the absorption system increases, the heating fluid, chilled water and cooling water flow rates are increased. This is because when the heat source temperature increases, the solar heat gain will increase and hence more transferable fluid flow rate is required in order to deliver this amount of heat. In addition, the increase in the heat gain results in an increase in the refrigerant vapor produced and hence more cooling water in condenser is required in order to condense that amount of refrigerant vapor.

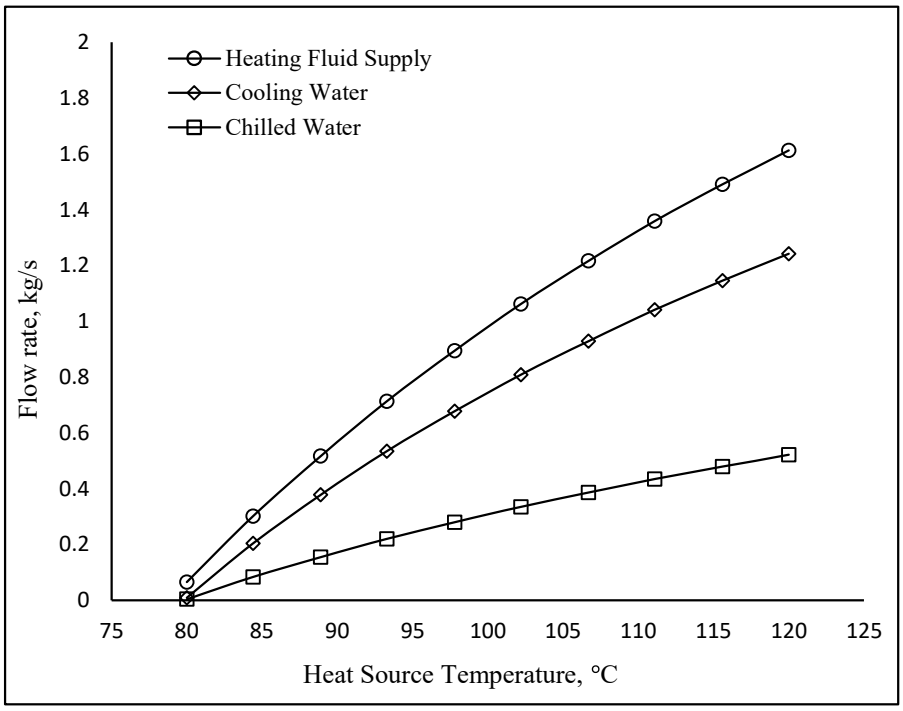

Figure 3. 9 : Effect of heat source temperature on condenser cooling water flow rate and evaporator chilled water flow rate

3.3.2 Validation

In order to support the developed model, Results of the present study are compared with results obtained using TRNSYS program Balghouthi et al. (2008) [51] for the same cooling capacity of 11 kW. The operating conditions are 84.6, 4.4, 38, 36.2, 0.6, 0.561, 0.613 for generator, evaporator, condenser and absorber temperatures, solution heat exchanger effectiveness, strong solution concentration and weak solution concentration, respectively.

The COP and the heat transfer rates of the condenser obtained from the two programs are presented in Table 3. The results for strong, weak solutions and refrigerant mass flow rates from TRNSYS software are also presented in Table 3.3 for sake of comparison. The simulation results for the two programs show that, only 2.03% is observed as a maximum percentage difference between the two programs.

Table 3. 4 : Results obtained from the EES and TRBSYS programs

Parameter	**Present study (EES)**	**Published study (TRNSYS)** [51]	**Percentage difference (%)**
COP	0.725	0.74	2.03
Condenser (kW)	11.7	11.89	1.6
Weak solution mass flow rate (kg/s)	0.0552	0.056	1.43
Strong solution mass flow rate (kg/s)	0.0505	0.0512	1.37
Refrigerant mass flow rate (kg/s)	0.0047	0.0048	2.1

The developed model was also validated and supported against experimental results of Gonzalez et al. (2011) [52]. The main input parameters which were used in the experimental work are cooling power, generator temperature, condenser temperature, absorber temperature, evaporator temperature and heat exchanger effectiveness and the values considered are 4.5 kW, 87.5 °C, 41 °C, 36 °C, 7.5 °C and 0.865, respectively.

The comparison shows that the results of the heat rates of generator and absorber and COP are acceptable. The comparison in Table 3.5 shows a maximum percentage difference of 11.7% in COP.

Table 3. 5 : Results obtained from the developed model and the experimental work

Parameter	**Present study (EES)**	**Published study (Exp.)** [52]	**Percentage difference (%)**
COP	0.795	0.9	11.7
Absorber (kW)	5.377	5.0	7.54
Generator (kW)	5.663	5.5	2.96

CHAPTER 4

DIRECT CONTACT MEMBRANE

DISTILLATION SYSTEM

4.1 Mathematical Modelling of DCMD System

4.1.1 Mass Transfer

Fig. 4.1 shows a configuration of direct contact membrane distillation (DCMD) module. In DCMD module, a hot fluid (hot stream) is run over a hydrophobic membrane. On the other side of the membrane, fluid (cold permeate) flows.

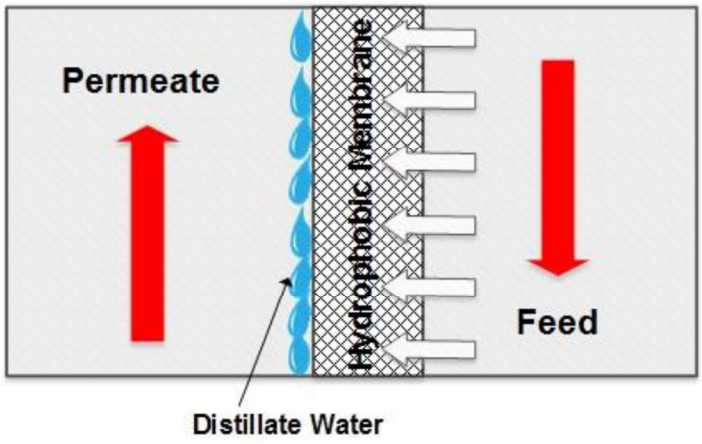

Figure 4. 1 : Schematic of DCMD Process

Due to temperature difference on the membrane surfaces, a difference of vapor pressure is produced across the membrane that causes water vapor formed in the feed side (due to high temperature) to cross the membrane and condense on the permeate side. The permeate mass flux through the membrane depends mainly on equivalent diffusion coefficient and the difference of vapor pressure of water in both feed and permeate sides. The permeate mass flux can be given as [53], [54], [55]:

$$J_w = D_e * \Delta P_m = D_e * (P^{\circ}_{wf} - P^{\circ}_{wp}) \tag{4.1}$$

Where J_w is the mass flux of permeate, and D_e is the equivalent diffusion coefficient. ΔP_m is the vapor pressure difference at transmembrane surfaces. P°_{wf} and P°_{wp} are the vapor pressures of feed and permeate sides at the membrane surfaces; respectively. They can be calculated using the Antoine equation as follows:

$$P^{\circ}_{wf} = exp\left[(23.1964) - \frac{3816.44}{T_{mf} - 46.13}\right] \tag{4.2}$$

$$P^{\circ}_{wp} = exp\left[(23.1964) - \frac{3816.44}{T_{mp} - 46.13}\right] \tag{4.3}$$

Essalhi et.al. [54] considered the concept of combined (Knudsen and molecular) diffusions by introducing a factor α which is the ratio of Knudsen diffusion to mass diffusion and tells the dominance of phenomenon which is occurring in mass transfer. The value of α can vary between 0 to 1 [54].

$$D_e = \left[\left(\frac{\propto}{D_k}\right) + \left(\frac{1-\propto}{D_m}\right)\right]^{-1} \tag{4.4}$$

D_k and D_m represents Knudsen and molecular diffusion coefficients respectively, and can be found by the following expressions [54].

$$D_k = \left[\left(\frac{3 * \delta * \tau}{2 * \varepsilon * d_{pore}}\right) + \left(\frac{\pi * R * T_m}{8 * M_w}\right)^{0.5}\right]^{-1} \quad (4.5)$$

$$D_k = \left[\left(\frac{R * T_m * \delta * \tau * P_{air,pore}}{M_w * \varepsilon * PD_{w,a}}\right)\right]^{-1} \quad (4.6)$$

Where δ is membrane thickness, ε is membrane porosity, R is universal gas constant, T_m is the mean or average temperature across membrane surfaces, d_{pore} is the pore diameter that is measured in accordance with the membrane tortuosity factor, M_w is the molecular weight of water molecules, P is the total pressure, and $D_{w,a}$ is pressure independent molecular diffusion coefficient for water and air or simply $D_{w,a}$ is diffusivity of water vapors in air.

τ is the membrane tortuosity which represents the deviation of pore shape from circular to elliptical. Tortuosity depends upon the shape and looseness of pores. Two different relations are commonly used to calculate tortuosity. Andrjesdóttir et al. and Essalhi et al. [54], [56], [57] used the following expression to calculate tortuosity;

$$\tau = \frac{1}{\varepsilon} \quad (4.7)$$

Although both expressions do not show much variation in flux predictions, they can be used depending upon the membrane manufacturing method. Diffusivity of water vapors produced through the static air inside the membrane pores can be calculated as [57], [58], [59]:

$$PD_{w,a} = 1.895 * 10^{-5} * T_m^{2.072} \quad (4.8)$$

Where T_m is the mean or average temperature across the membrane surfaces. It can be expressed as:

$$T_m = \frac{T_{mf} + T_{mp}}{2} \quad (4.9)$$

4.1.2 Heat Transfer

Referring to DCMD configuration in fig. 1, different modes of heat transfer are identified. In the feed side, fluid is at high temperature and high salinity flowing over the membrane surface. The heat transfer rate in this side will be due to convection. Then, on the permeate side, the fluid is flowing, causing convective heat transfer to occur. However, in the membrane pores due to mass flux, the heat transfer is due conduction and mass flux. So heat transfer in a DCMD module is occurring in three regions.

1- Convective heat transfer in the boundary layer region from the feed stream to membrane surface. This heat transfer mechanism can be written using Newton's law of cooling [54], [58], [60]:

$$Q_f = h_f * (T_{bf} - T_{mf}) \tag{4.10}$$

Where T_{bf} and T_{mf} are the bulk feed temperature and membrane surface temperature in the feed side respectively. h_f is the convective heat transfer coefficient in feed side that can be calculated by using different correlations depending on the flow type (laminar or turbulent).

2- Heat transfer through membrane material by conduction and through the pores by evaporative mass flux through the membrane.

Heat carried by the vapors (Evaporative heat transfer) is written as product of vapor mass flux (J_w) and enthalpy of vaporization (ΔH_v);

$$Q_v = J_w * \Delta H_v \tag{4.11}$$

The Enthalpy of vaporization of water is expressed as [25]:

$$\Delta H_v = \left[\left(1.7535 * T_{mf}\right) + 2024.3\right] \quad (4.12)$$

Where T_{mf} is the temperature of the membrane surface at feed side.

Conductive heat transfer through membrane matrix can be represented by using Fourier's law of conduction as:

$$Q_c = \left(\frac{k_m}{\delta}\right) * (T_{mf} - T_{mp}) \quad (4.13)$$

Where T_{mf} and T_{mp} are membrane surface temperatures in feed and permeate side respectively. δ is membrane thickness and k_m is effective thermal conductivity of membrane.

The total heat transfer across the membrane is simply the addition of the conductive and evaporative heat transfer through the membrane.

$$Q_m = Q_c + Q_v \quad (4.14)$$

3- Convective heat transfer in the boundary layer region from membrane surface to bulk permeate side and can be given as:

$$Q_p = h_p * (T_{mp} - T_{bp}) \quad (4.15)$$

Where T_{mp} is membrane surface temperature at permeate side, T_{bp} is bulk permeate vapor temperature. h_p is the convective heat transfer coefficient in permeate side that can be calculated by using different correlations.

Under steady state condition, the following conservation of energy, the heat transfer through feed, membrane and permeate side are equivalent.

$$Q_f = Q_m = Q_p \tag{4.16}$$

Therefore, when the above condition is fulfilled, the temperatures of the membrane surfaces at feed and permeate sides can be calculated [54], [61]:

$$T_{mf} = \frac{k_m * \left(T_{bp} + \frac{h_f}{h_p} * T_{bf}\right) + \left[\delta * (h_f * T_{bf} - J_w * \Delta H_v)\right]}{k_m + \left[h_f * \left(\delta + \left(\frac{k_m}{h_p}\right)\right)\right]} \tag{4.17}$$

$$T_{mp} = \frac{k_m * \left(T_{bf} + \frac{h_p}{h_f} * T_{bp}\right) + \left[\delta * (h_p * T_{bp} - J_w * \Delta H_v)\right]}{k_m + \left[h_p * \left(\delta + \left(\frac{k_m}{h_f}\right)\right)\right]} \tag{4.18}$$

4.1.3 Calculation of Convection heat transfer coefficient (h)

By definition of convective heat transfer coefficient, h:

$$h = \frac{Nu * k}{D_h} \tag{4.19}$$

Where k is the average thermal conductivity of fluid in feed or permeate and D_h is the hydraulic diameters of flow channels and Nu is Nusselt number. In case of turbulent flow, the Nusselt number [54], [62] of the feed (Hot side) and permeate (cold side) streams can be given as:

$$Nu_f = 0.027 * \left(Re_f\right)^{0.8} * \left(Pr_f\right)^{0.4} * \left[\left(\frac{\mu_{bf}}{\mu_{mf}}\right)\right]^{0.14} \tag{4.20}$$

$$Nu_p = 0.027 * \left(Re_p\right)^{0.8} * \left(Pr_p\right)^{0.33} * \left[\left(\frac{\mu_{mp}}{\mu_{bp}}\right)\right]^{0.14} \quad (4.21)$$

Where *Re* is Reynolds number of bulk feed and permeate in the feed and permeate channel, respectively. μ_{bf} and $\mu_{bp}$is the dynamic viscosity of bulk feed stream. μ_{mf} and $\mu_{mp}$is the viscosity of feed at the membrane surface.

Pr_f and Pr_p is Prandtl number of bulk feed and permeate in the feed and permeate channel, respectively. Prandtl number is the ratio of viscous diffusion rate to thermal diffusion rate and can be written as:

$$Pr = \frac{v}{\propto} = \frac{\mu * c_p}{k} \quad (4.22)$$

Where μ is the dynamic viscosity, *k* is the thermal conductivity, and C_p is the specific heat of the fluid. In case of laminar flow, Graetz-Lévéque introduced the following correlation for Nusselt Number [63], [64]:

$$Nu = 1.86 * \left(\frac{Re * Pr * D_h}{L}\right)^{0.33} \quad (4.23)$$

D_h is the channel hydraulic diameter, L is the channel length.

4.2 Results and Discussion

4.2.1 Steady State Modelling

In order to simulate the mass, heat transfer and performance equations of DCMD system, the membrane properties and geometrical constants listed in Table 1 are used. The DCMD system modeling is carried out using Engineering Equation Solver (EES) [50]. The software is used to conduct the thermodynamic analysis of DCMD system and predict the permeate flux & all heat transfer rates.

Table 4. 1 : Membrane Properties and Geometrical Constant Used

	Parameter	Symbol	Units	Value
1	Membrane thickness	δ	µm	154
2	Porosity	ε	–	0.88
3	Thermal conductivity of gas filling the pores	k_g	W/mK	0.0227
4	Thermal conductivity membrane material	k_{mem}	W/mK	0.25
5	Pore size	d_p	µm	0.45
6	Gas constant	R	J/Kmol	8.314
7	Channel width	W	mm	25
8	Channel depth	H	mm	5
9	Channel length	L	mm	66

The effect of feed temperature on the permeate flux is studied over a range of temperatures from 40 °C to 80 °C while the range of 5 °C to 25 °C is considered to examine the effect of cold permeate temperatures. Furthermore, the effect of feed and coolant flow rates on permeate flux is studied over the range 0.25 to 0.75 kg/s and all the results are obtained in Figs. 4.2 and 4.3.

Figs. 4.2 illustrates the effect of feed temperature and flow rate on the permeate flux. As illustrated in the figure, there is a gradual increase in the permeate flux when the feed temperature increases. This is due to an increase in the evaporation rate which is enhanced as the feed temperature increases. Furthermore, It is clear that the permeate flux increases with increase in feed flow rate. This is due to the fact that as the feed flow rate increases, high mixing effect occurs inside the feed channel due to higher turbulence generated and as a result increase the flux.

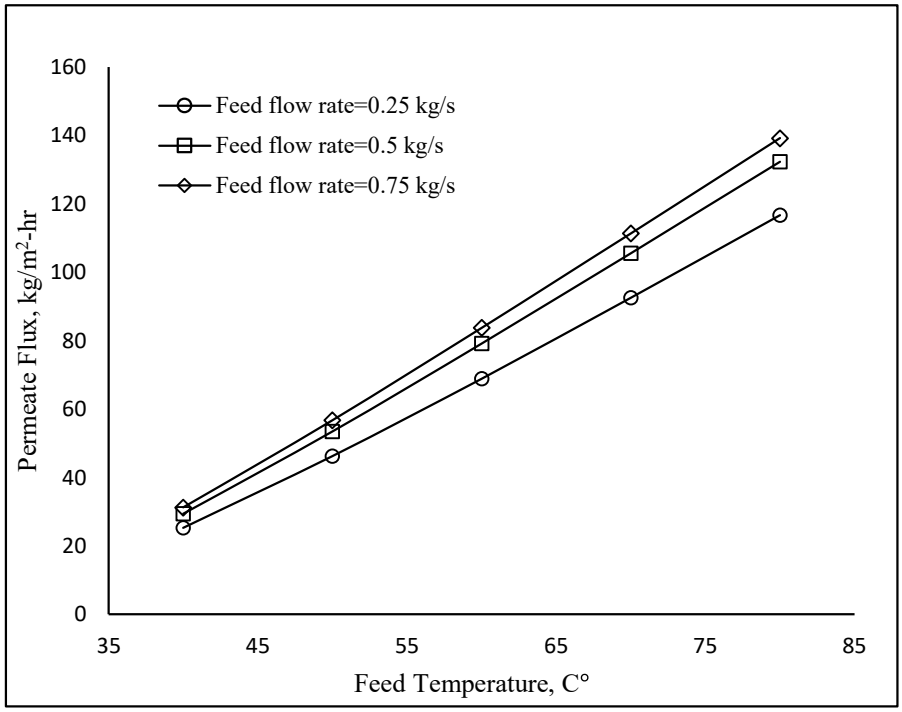

Figure 4. 2 : The effect of feed temperature and flow rate on flux. Coolant temperature = 25 °C & coolant flow rate = 0.25 kg/s

Figure 4.3 illustrates the effect of coolant temperature and flow rate on the system permeate flux. The permeate flux decreases with increase in coolant temperature. This is because when the coolant temperature increases, the temperature difference between the coolant and the feed chambers decreases. The decrease in the temperature difference represent a reduction in the potential for condensation, which leads to a decrease in the flux. Additionally, as observed from the figure, the permeate flux increases as the coolant flow rate increases. However, increasing the feed flow rate is more effective on system productivity as compared to the effect of increasing the coolant flow rate because it is the source vaporization and controlling the permeation process.

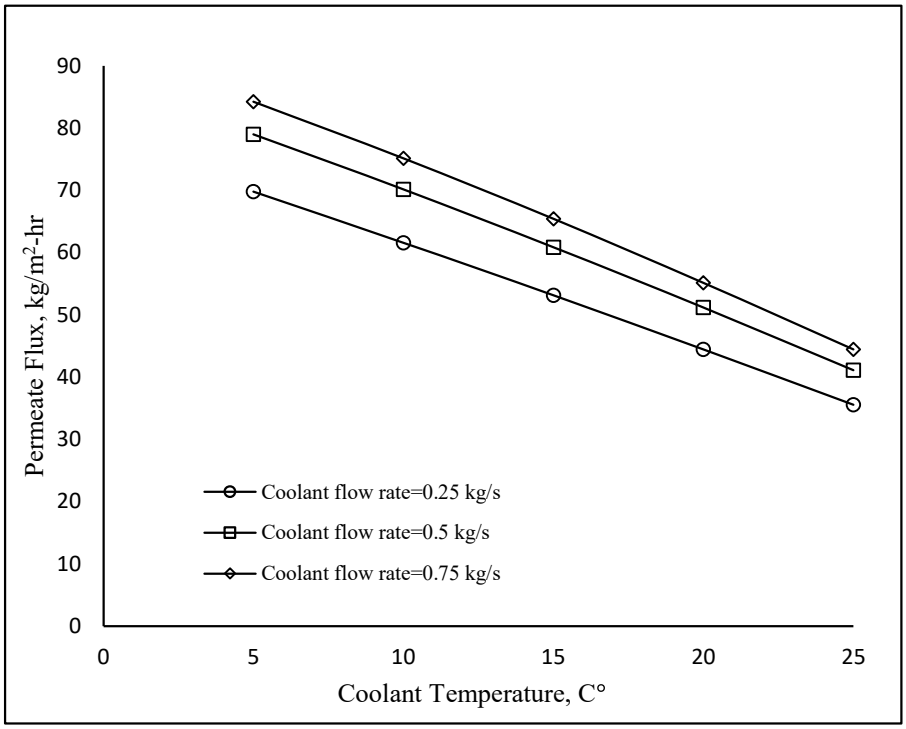

Figure 4. 3 : The effect of coolant temperature and flow rate on flux. Feed temperature = 45 °C & feed flow rate = 0.25 kg/s

4.2.2 Validation

To examine the flux prediction capability of the theoretical model, the developed model is validated against the experimental work of Khalifa et al [31]. The membrane properties and the geometrical constants used are tabulated in Table 4.2. Figs. (4.4 to 4.6) illustrate the effects of increasing coolant temperature, feed flow rate and feed temperature respectively for both studies.

Table 4. 2 : Membrane Properties & Geometrical Constant

Symbol	**Values as used in** [31]
$\boldsymbol{\delta}$	7
$\boldsymbol{\varepsilon}$	0.8
$\boldsymbol{d_p}$	0.45
R	8.314
L	66
W	24
H	5
A	6.192×10^{-3}

Fig. 4.4 illustrates the permeate flux vs. feed temperature in DCMD for the developed model and experiment of Khalifa et. al. [31]. The coolant temperature is fixed at 21 °C, coolant flow rate is 3.65 L/min and feed flow rate is 4.6 L/min. Fig. 4.5 illustrates the permeate flux vs. coolant temperature in DCMD for the developed model and experimental results. The feed temperature is fixed at 60 °C, coolant flow rate is 3.65 L/min and feed flow rate is 4.6 L/min. The maximum percentage error between the experimental and theoretical work are 9% and 3.9% obtained in Fig. 4.4 and Fig. 4.5, respectively.

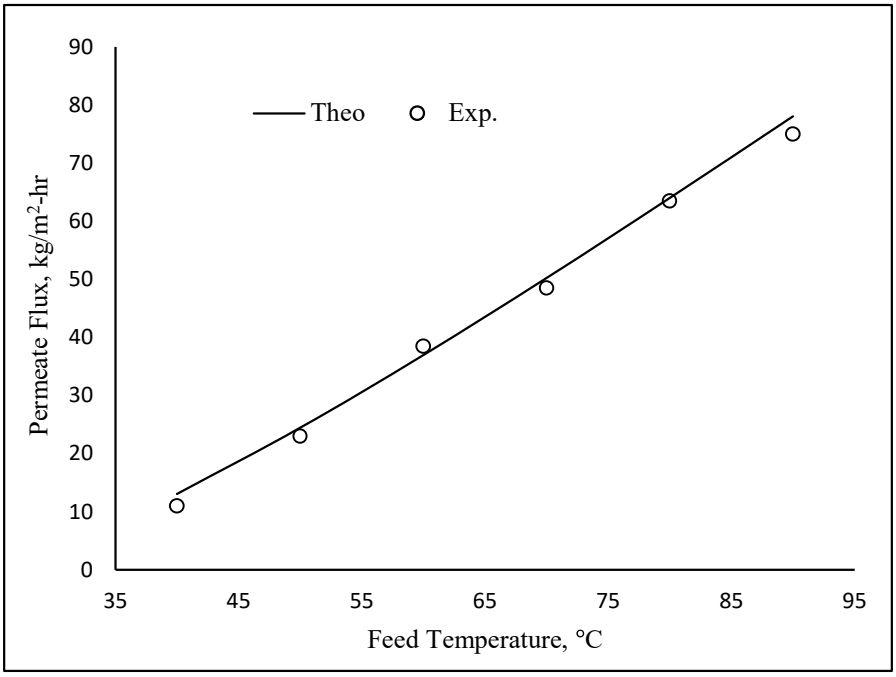

Figure 4. 4 : The effect of feed temperature on flux

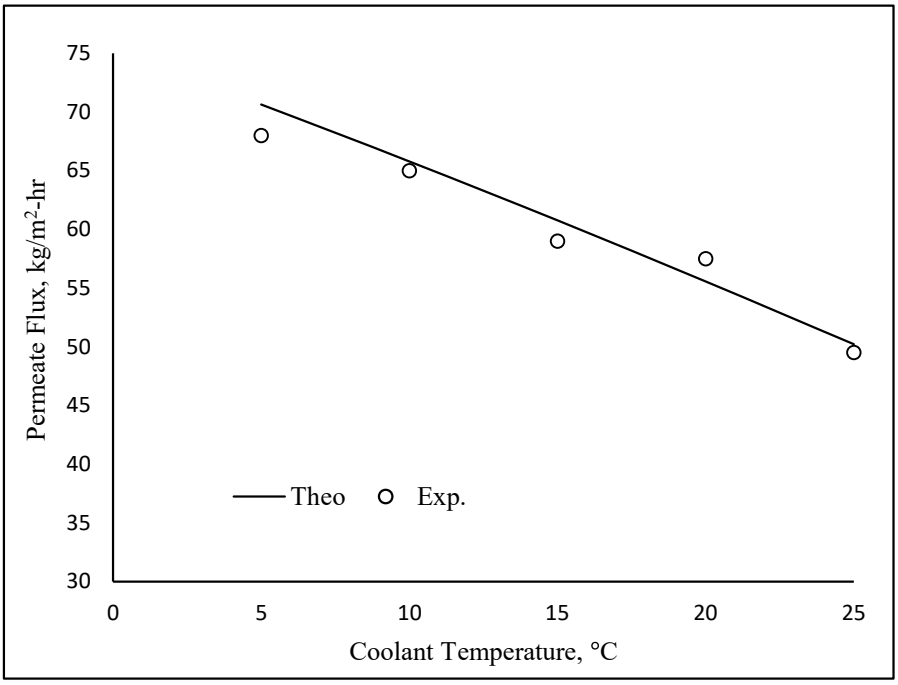

Figure 4. 5 : The effect of coolant temperature on flux

Fig. 4.6 illustrates the permeate flux vs. feed flow rate temperature in DCMD for the developed model and experimental results. The feed and coolant temperatures are fixed at 60 and 21 °C respectively and coolant flow rate is 3.65 L/min. However, the results show good agreement between the experimental results and the present model prediction. The maximum percentage error obtained is 3%.

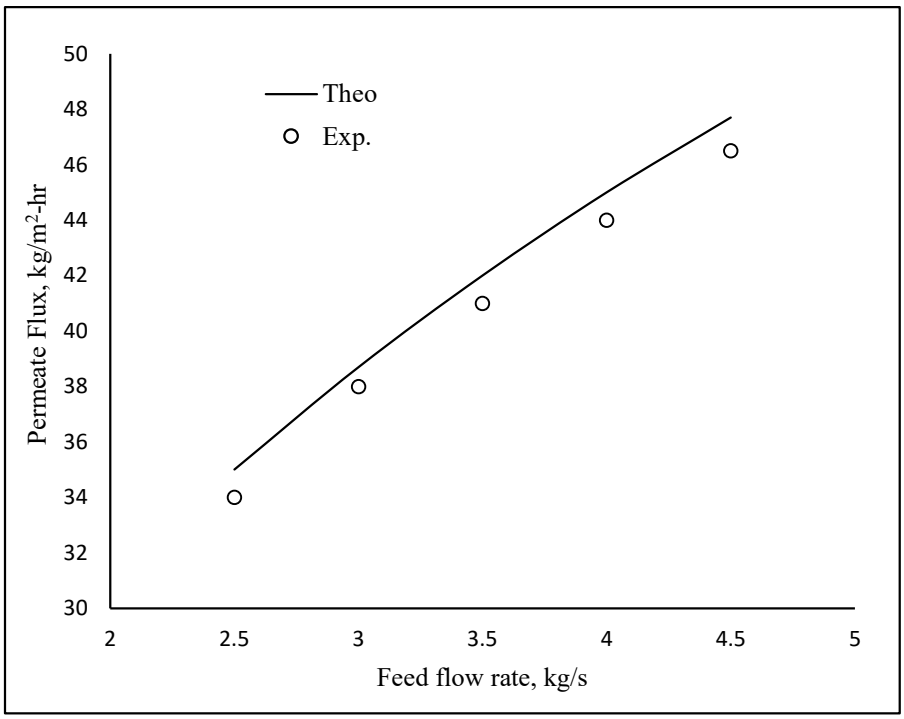

Figure 4. 6 : The effect of feed flow rate on flux

CHAPTER 5

COMBINED SOLAR ABSORPTION AND MEMBRANE DISTILLATION SYSTEMS

This chapter presents the design of the proposed integrated solar (LiBr-water) absorption and direct contact membrane distillation (DCMD) system, as well as the modifications conducted to improve the desalination yield.

5.1 Introduction

The production of fresh water and chilled water for drinking and air conditioning purposes usually consume large amounts of energy (electricity or thermal). When the capacities of water production facilities are large; the heat and power required can only be provided by thermal power plants. In air conditioning area, a similar development is taking place where centralized district cooling plants are remarkably replacing roof top, local chillers or window units.

Integrated systems that simultaneously produce two or more products are usually cost effective and more energy-efficient compared to separate single-product systems that are generating the same products. Therefore, using these integrated systems have become attractive and successful with the use of one of the renewable energy resources such as

solar energy. Many absorption refrigeration processes use solar energy to produce chilled water for the air-conditioning purpose. Heat from these processes is then rejected as a waste heat to the surrounding. This waste heat can be converted to useful energy by using one of the thermal desalination systems, such as membrane distillation system. Hence, these systems/technologies can play an important role in solving the water shortage as well as the high summer temperature problems, such as in Dammam, Saudi Arabia. In this study, the concept of combination of solar cooling and thermal desalination systems is discussed.

5.2 Detailed Description of the Integrated System

Figure 5.1 diagrammatically illustrates a hybrid LiBr-water solar absorption cycle combined with a direct contact membrane distillation system. The proposed system is composed of 3 main sub-systems. These subsystems are labelled in Fig. 5.1 as: (A) the membrane distillation sub-system, (B) the absorption cooling sub-system, and (C) the solar collection sub-system.

5.2.1 Absorption Cooling Sub-System (A)

It is composed of a traditional single-effect ($LiBr–H_2O$) absorption refrigeration cycle; which includes a generator, an absorber, expansion valves, an evaporator and other components such as the solution pump, and the solution heat exchanger, as discussed in chapter 3. The condenser of the absorption system is now replaced by a feed heat exchanger (FHX) which is used to condense the refrigerant vapor in the hot side in order to complete the cooling cycle and to heat up the cooling water in order to be fed into the membrane distillation system. Solar energy is used to drive the absorption cycle so that heat is supplied to the generator as thermal energy.

5.2.2 Membrane Distillation Sub-System (B)

The proposed desalination system is the direct contact membrane distillation (DCMD) system. It is clear that the two subsystems (system A and B) are linked together through the two sides of the membrane distillation unit, which is direct contact membrane distillation (DCMD) unit.

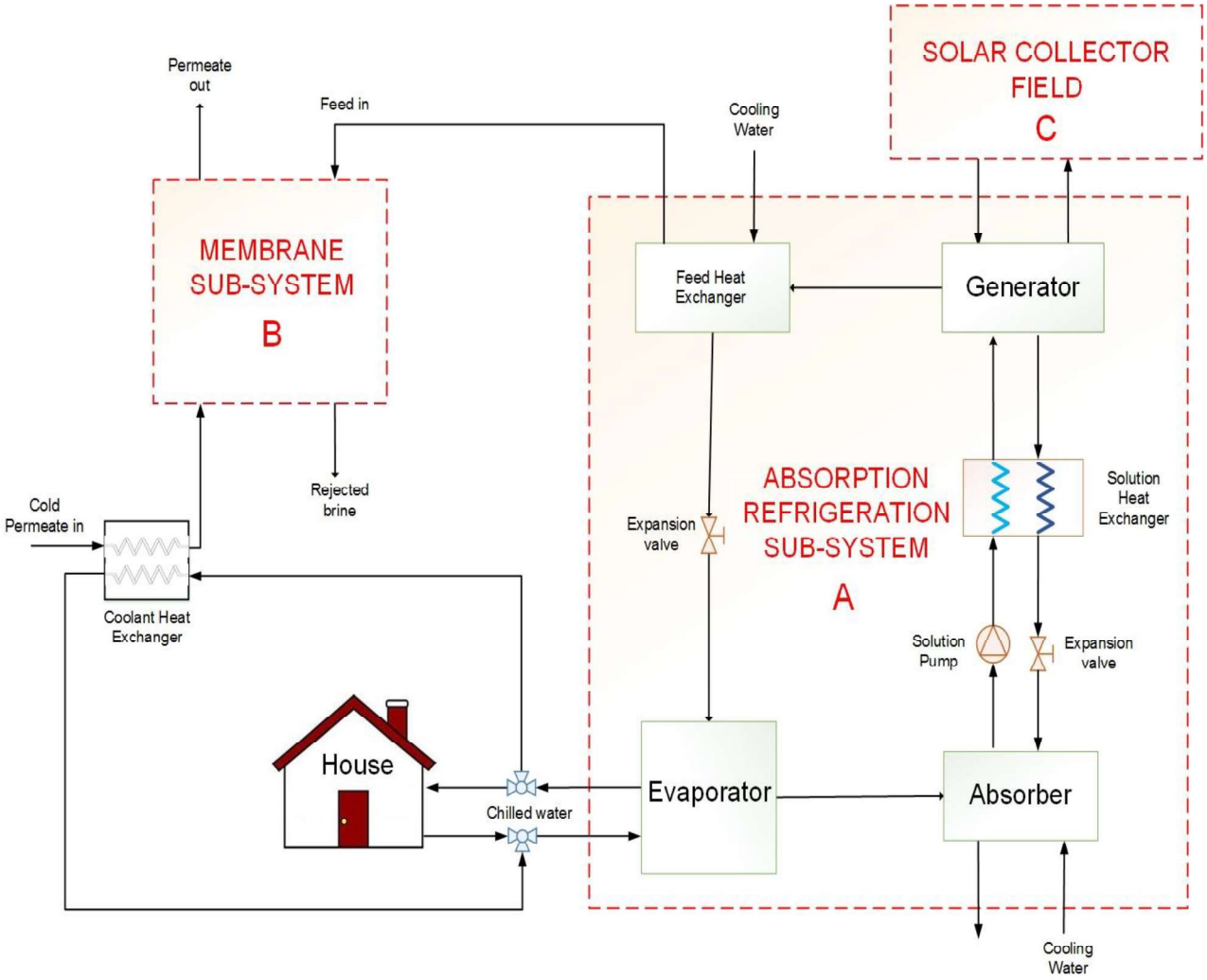

Figure 5. 1 : Integrated Solar Cooling and Desalination System

In DCMD, the membrane surfaces are in direct contact with two solution streams, which are in different temperatures. A considerable amount of cooling water that is rejected from the feed heat exchanger of the absorption system (hot water) is fed into DCMD system. At

the membrane interface, vapor in the hot feed is formed on the hot side of the membrane diffuses through the membrane pores and the remaining liquid exits as brine. The permeate side of membrane is maintained colder by means of a coolant stream (in case of DCMD, this coolant should be distillate water). So, permeated vapor condenses at the permeate side of the membrane. It is then collected as a distillate water.

5.2.3 Solar Collector Sub-System (C)

It consists of conventional evacuated tube solar collectors, which are used to drive the absorption cycle. Among the commercially available solar collectors, evacuated tube collectors would be a suitable choice as they are able to operate up to 100 °C. Nevertheless, other collectors with lower/higher maximum temperatures could also be chosen. However, capital and operating cost, local weather conditions, solar field size, and maintenance and operation costs should be considered in the final selection.

The proposed combined system has two useful outputs: sensible cooling effect and fresh water, while the system inputs are the solar heat gain as well as the solution pump work. In this case, the performance definition is not suitable because the two products have different units and physical meaning. So, a definition should be developed in terms of heat transfer rate for both fresh water production and cooling effect. Therefore, the overall efficiency of the proposed integrated system is defined as:

$$E_{overall} = \frac{\dot{Q}_e + (\dot{Q}_v)}{\dot{Q}_g + \dot{W}_p} \tag{5.1}$$

Where $\dot{Q}_e$ is the cooling effect, $\dot{Q}_v$ is the evaporative heat carried by distillate water, $\dot{Q}_g$ is the input heat to generator and $\dot{W}_p$ is the solution pump work.

5.3 Combined System Configurations

In order to analyze the steady state performance of the proposed integrated solar absorption cooling and direct contact membrane distillation system, three configurations have been suggested for the integrated system:

5.3.1 Configuration A

Fig. 5.2 illustrates the first arrangement of the proposed integrated solar cooling and desalination system. This arrangement is aimed to simultaneous production of fresh water as well as cooling effect. In this arrangement, the rejected cooling water (hot feed), represented by ($\dot{m}_{16}$), from the feed heat exchanger (FHX) is fed into the feed side of the DCMD unit while distillate cooling water ($\dot{m}_{19}$), at 25 °C is fed into the permeate side of the DCMD unit for condensation purposes. On the hand, the produced chilled water ($\dot{m}_{17}$), at 5 °C is used to fulfill the cooling requirements of the house.

The feed heat exchanger (FHX) considered in this arrangement is a shell and tube heat exchanger. The heat transfer rate between the refrigerant vapor (hot side), represented by ($\dot{m}_7$), and the cold seawater (cold side), represented in label ($\dot{m}_{15}$), is governed by the temperature gradient and the mass flow rates. In steady state condition, the heat transfer rate of the hot side fluid must equal the heat transfer rate of the cold side fluid.

Therefore, in order to model the feed heat exchanger (FHX), the heat transfer rate equation for both sides should be calculated. The energy balance equation for the hot side is described by the following equation:

$$Q_{hot} = \dot{m}_7 \, C_{p_h} \, (T_7 - T_8) \tag{5.2}$$

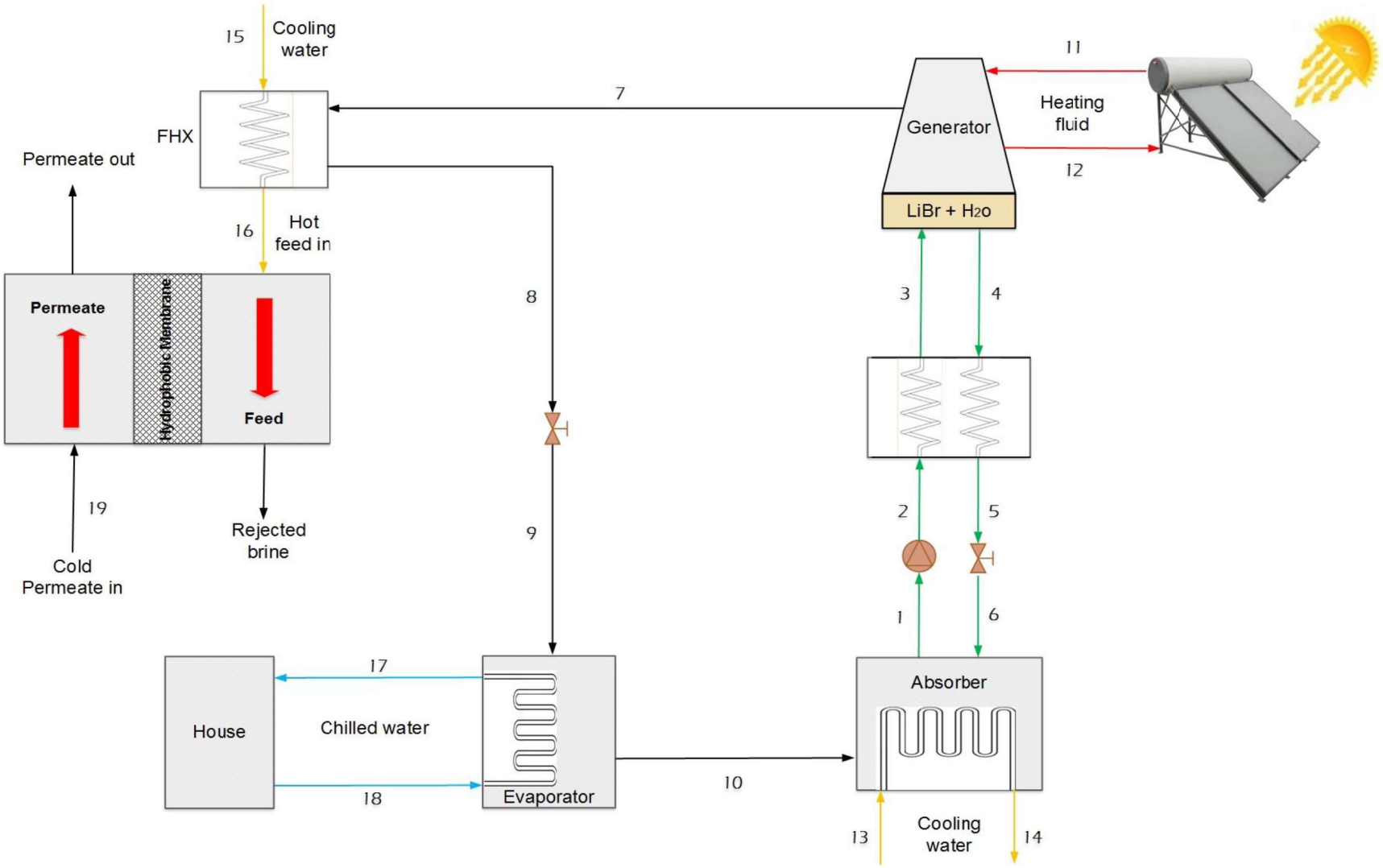

Figure 5. 2 : Configuration (A) for the integrated solar cooling and desalination system

Where $\dot{m}_7$ is the mass flow rate of refrigerant vapor, C_{p_h} is the specific heat transfer rate of the refrigerant (water), T_8 is the outlet temperature and T_7 is the inlet temperature. The energy balance equation for the cold side is described by the following equation:

$$Q_{cold} = \dot{m}_{15}\, C_{p_c}\, (T_{16} - T_{15}) \tag{5.3}$$

where $\dot{m}_{15}$ is the mass flow rate of cooling water, C_{p_c} is specific heat transfer rate of cooling water, T_{16} is the outlet temperature and T_{15} is the inlet temperature.

5.1.2 Configuration B

Fig. 5.3 presents another arrangement of proposed integrated cooling and desalination system. This arrangement is aimed to increase the fresh water productivity for DCMD unit by maintaining a low temperature at the permeate side of the membrane distillation unit while meeting the cooling requirements of the house. However, this improvement will be applied at the time when the cooling load of the house is reduced (e.g. in winter season), such that partial chilled water is needed for the house cooling requirements.

In this arrangement, the two sub-systems, absorption cooling and membrane distillation, are linked through the two sides of DCMD unit. In one side, the rejected cooling water (hot feed) represented by ($\dot{m}_{16}$) from the feed heat exchanger (FHX) is fed into the feed side of the DCMD unit. In the other side, the chilled water represented in label ($\dot{m}_{17}$) produced from the evaporator is divided (under controllable bypass percentages) into two paths:

(1) Path 1, this branch of chilled water ($\dot{\boldsymbol{m}}_{20}$), passes to the typical house to fulfill the daily cooling requirements.

(2) Path 2, this branch of chilled water ($\dot{m}_{21}$), passes to the coolant heat exchanger (CHX) to cool down the permeate which is later fed into the permeate side of DCMD unit.

However, there are two 3-way valves in this arrangement. Valves V_1 and V_2 are used to distribute the chilled water between the coolant heat exchanger and the typical house. The coolant heat exchanger (CHX) considered in this arrangement is a shell and tube heat exchanger. The heat transfer rate between the chilled water (cold side), represented by ($\dot{m}_{21}$), and the permeate of DCMD unit (hot side), represented by ($\dot{m}_{19}$), is governed by the temperature gradient and the mass flow rates. In steady state, the heat transfer rate of the hot side fluid must equal the heat transfer rate of the cold side fluid.

Therefore, in order to model the coolant heat exchanger (CHX), the heat transfer rate equation for both sides should be calculated. The energy balance equation for the cold side is described by the following equation:

$$Q_{cold} = \dot{m}_{21}\, C_{p_c}\, (T_{22} - T_{21}) \tag{5.4}$$

where $\dot{m}_{21}$ is the mass flow rate of the chilled water branch, C_{p_c} is the specific heat transfer rate of the chilled water, T_{22} is the outlet temperature and T_{21} is the inlet temperature. The energy balance equation for the hot side is described by the following equation:

$$Q_{hot} = \dot{m}_{19}\, C_{p_h}\, (T_{19} - T_{24}) \tag{5.5}$$

Where $\dot{m}_{19}$ is the mass flow rate of the permeate, C_{p_h} is the specific heat transfer rate of the permeate, T_{24} is the outlet temperature and T_{19} is the inlet temperature.

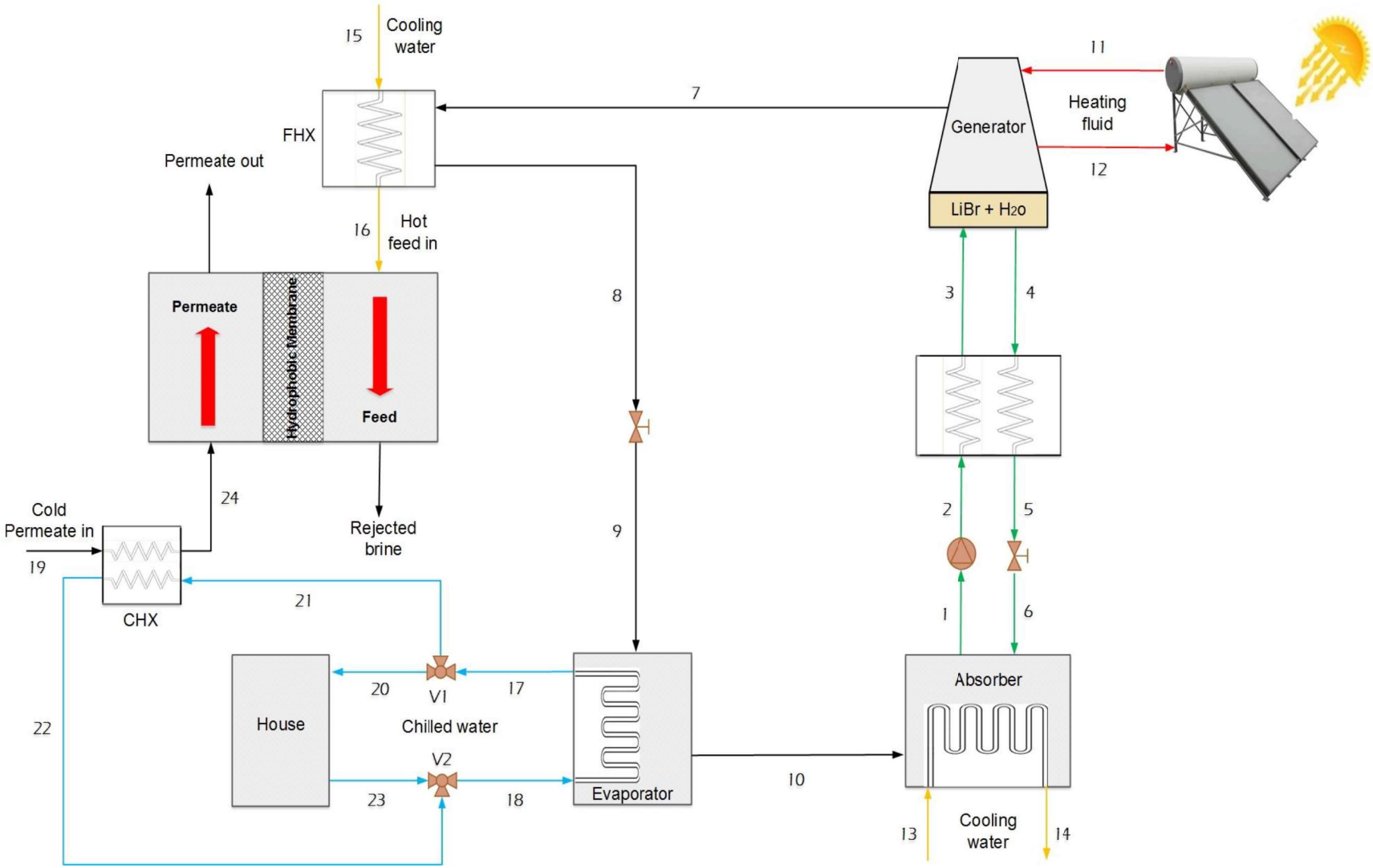

Figure 5. 3 : Configuration (B) for the integrated solar cooling and desalination system

5.1.3 Configuration C

Fig. 5.4 illustrates the third arrangement of the proposed integrated solar cooling and desalination system. This arrangement is aimed to increase the fresh water productivity for DCMD unit by maintaining a low temperature at the permeate side of the membrane distillation unit. Therefore, the waste heat form the absorption system is considered as the thermal heat required to drive the membrane distillation system. Similarly, the cold side of the membrane distillation system is considered as the cooling load for the absorption system.

In this arrangement, the rejected cooling water (hot feed), represented by ($\dot{m}_{16}$), from the feed heat exchanger (FHX) is fed into the feed side of the DCMD unit while the chilled water produced from the evaporator ($\dot{m}_{17}$), at 5 °C is fed into the coolant heat exchanger (CHX) in order to cool down the permeate which is later introduced to DCMD unit to enhance the condensation process.

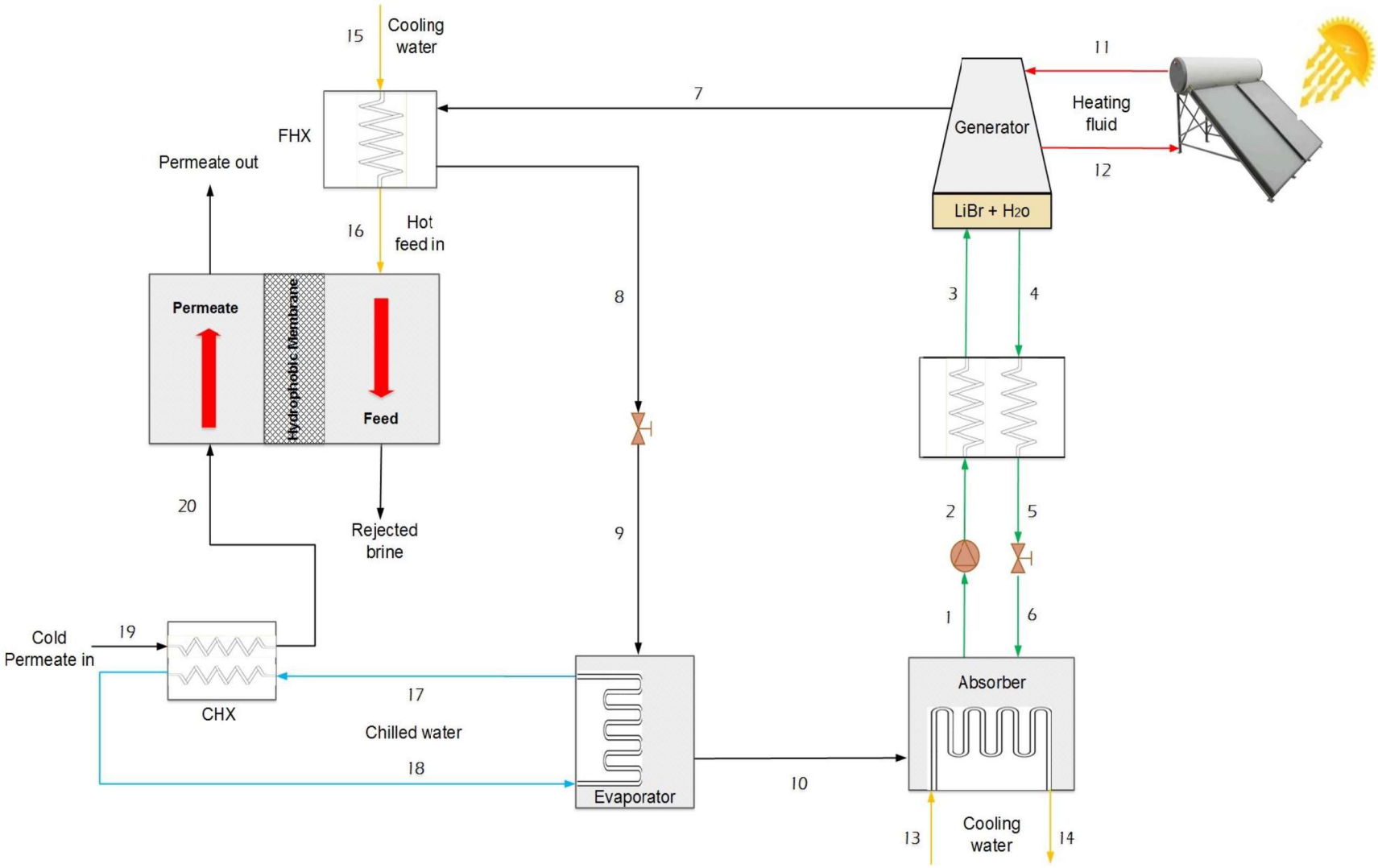

Figure 5. 4 : Configuration (C) for the integrated solar cooling and desalination system

5.4 Results and Discussion

To simulate the proposed combined system, a code based on combined physical models has been developed using Engineering Equations Solver (EES). The components of the sub-systems which are already designed in the previous chapters are used, under steady state operation and a nominal input thermal temperature of about 80 - 120 °C. The mass and energy equations are solved to determine the mass flow rate ($\dot{m}$) and enthalpy (h) for each of the thermodynamics states. This helps to analyze the overall system performance, cooling capacity and fresh water productivity based on given design data.

5.2.1 Arrangement (A)

The effect of heat source temperature on fresh water productivity, cooling capacity and overall integrated system performance is studied over a range of temperatures from 80 °C to 120 °C with an increment of 10 °C. For DCMD system, certain assumptions have been considered for flow conditions. The feed flow rate (cooling seawater), represented by ($\dot{m}_{15}$), that is introduced to feed heat exchanger (FHX) at 25 °C is varied from 4 l/min to 10 l/min, at each selected heat source temperature. The permeate flow rate ($\dot{m}_{19}$), that feed the permeate side of the membrane distillation system at 25 °C is assumed to be 6 l/min. Figures 5.5 and 5.8 report the results of this analysis.

Fig. 5.5 shows the feed flow rate vs. feed temperature at different heat source temperatures. It can be seen clearly that, at a certain heat source temperature, increasing the feed flow rate ($\dot{m}_{15}$) through the feed heat exchanger results in a decrease in the feed temperature (T_{16}) introduced to DCMD unit. This is because, for instance at 90 °C heat source temperature, a certain heat transfer rate is resulted in the hot side of FHX.

Therefore, by increasing the feed flow rate, the resulted feed temperature is reduced in order to equalize these amounts of heat in the cold side of the heat exchanger. Similarly, the same behavior is observed upon increasing the heat source temperature from 90 °C to 120 °C.

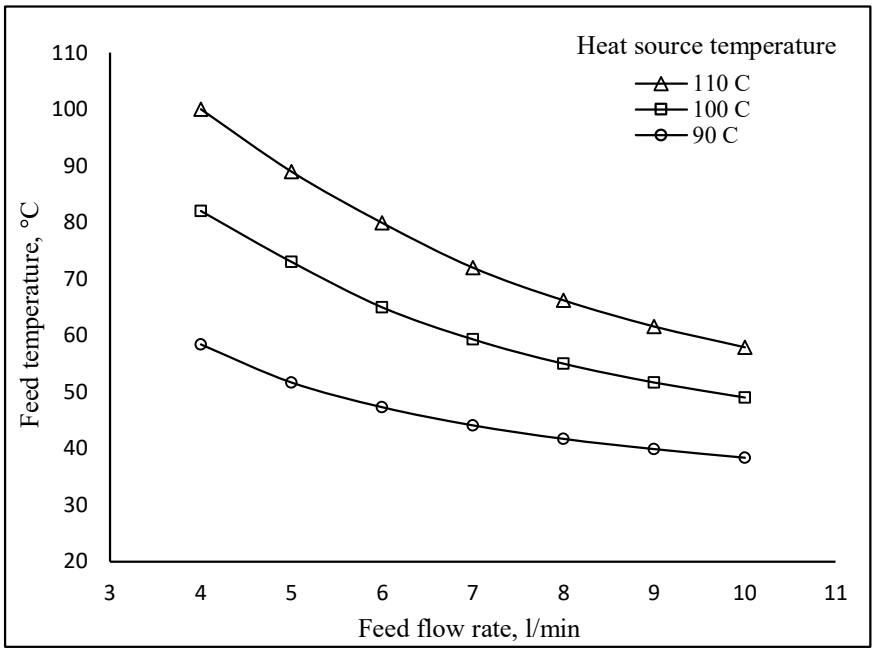

Figure 5. 5 : Effect of feed flow rate on feed temperature at different heat source temperatures.

Fig. 5.6 shows the effect of heat source temperature on fresh water productivity at different feed flow rates. Increasing the heat source temperature from 80 °C to 120 °C results in an increase in permeate flux obtained. This because the increase in heat source temperature results in an increase in water vapor produced from the generator and then more heat is rejected from the FHX in order to condense this amount of water vapor. The increase in amount of the heat rejected makes the feed water results at high temperature and hence increase the fresh water productivity as discussed in Fig. 4.4.

In addition, the effect of increasing the feed flow rate is illustrated. So, increasing the feed flow rate results in a decrease in water productivity. This due to, at each certain heat source

temperature (fixed amount of heat rejected from FHX), increasing the feed flow rate results in low feed temperature as introduced to DCMD unit.

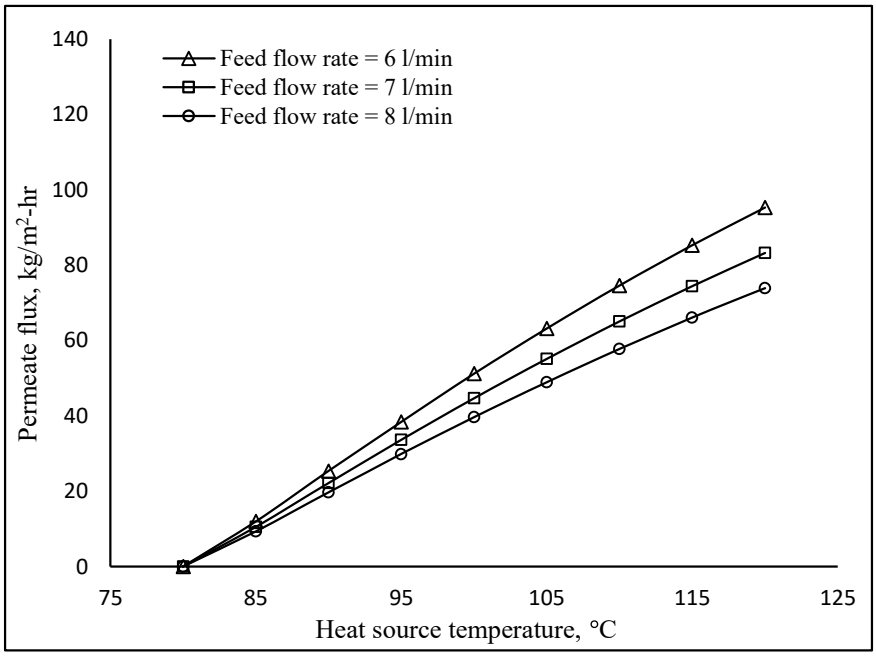

Figure 5. 6 : Effect of heat source temperature on fresh water productivity at different feed flow rates. Permeate flow rate = 6 l/min and permeate temperature = 25 °C.

Fig. 5.7 shows the effect of heat source temperature on produced cooling effect. As the heat source temperature increased, the cooling effect produced is also increased similar to the behavior discussed in Fig. 3.8. The maximum value recorded for cooling effect produced is 26 kW.

Fig. 5.8 shows the performance of the overall integrated system as a function of heat source temperature. As the input temperature increases, there is a rapid increase in overall efficiency up to 0.74, followed by a slower rate up to 0.76 to reach the maximum value around 0.774. Note that, in this arrangement, the integrated system has two output products which are cooling effect and fresh water. The significant increase in the efficiency is due to an increase in the cooling effect obtained compared to the system heat input. This

increment is later become proportional to the heat input and results to obtain the optimal value. However, the combination increase the overall efficiency compared to separated systems due to utilizing the waste/rejected in the form of heat recovery.

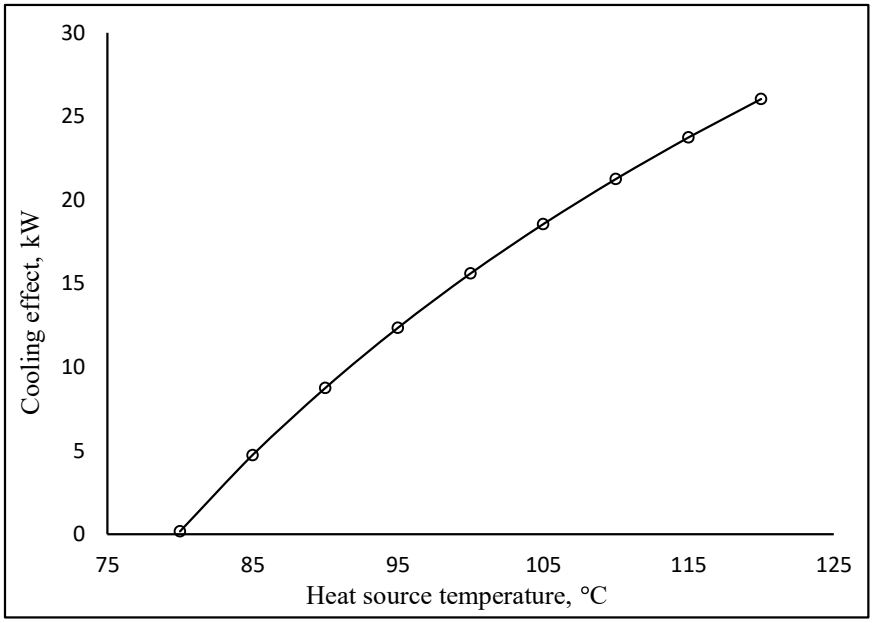

Figure 5. 7 : Effect of heat source temperature on produced cooling effect

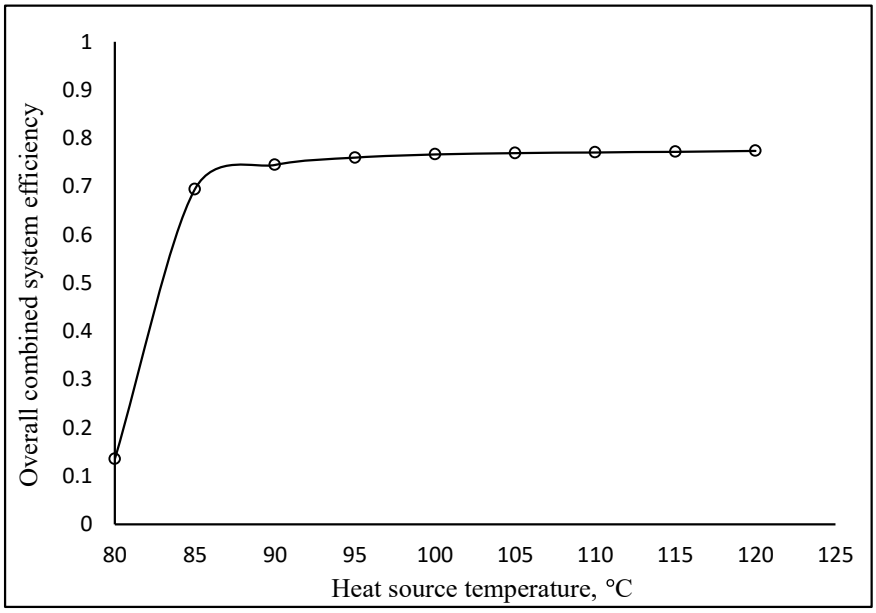

Figure 5. 8 : Effect of heat source temperature on overall integrated system efficiency. Feed flow rate = 6 l/min, permeate flow rate = 6 l/min and permeate temperature = 25 °C.

5.2.2 Arrangement (B)

In this arrangement, the effect of cooling load reduction in a typical house on fresh water productivity of DCMD system is presented. The effect of heat source temperature on fresh water productivity, cooling capacity and overall integrated system performance is studied over a range of temperatures from 80 °C to 120 °C with an increment of 10 °C. The reduction in the cooling load results in an increase in the branch of chilled water ($\dot{m}_{21}$) which introduced to coolant heat exchanger (CHX) that used to cool down the permeate of DCMD unit. Therefore, three bypass percentages are considered in order to study the effect of reducing the cooling load of the typical house. The bypass percentage is the percentage of branched chilled water flow rate into CHX ($\dot{m}_{21}$) divided by the total chilled water produced from the evaporator ($\dot{m}_{17}$).

For DCMD system, certain assumptions have been considered for flow conditions. The feed flow rate (cooling water), represented by ($\dot{m}_{15}$), that is introduced to feed heat exchanger (FHX) at 25 °C is assumed to flow at 6 l/min, at each selected heat source temperature. The permeate flow rate, represented by ($\dot{m}_{19}$), that is introduced to coolant heat exchanger (CHX) at 25 °C is varied from 4 l/min to 10 l/min, at each selected heat source temperature and bypass percentage. Figures 5.9 and 5.11 report the results of this analysis.

Figs. 5.9 and 5.10 show permeate flow rate vs. permeate temperature at 25 % and 50 % bypass percentages and different heat source temperatures. It can be seen clearly that, at a certain heat source temperature, increasing the permeate flow rate ($\dot{m}19$) through the coolant heat exchanger results in an increase in the permeate temperature (T_{24}) at the exit of heat exchanger as it flows to the DCMD unit. This is because, for instance at 90 °C heat

source temperature, a certain heat transfer rate is resulted in the cold side of CHX. Therefore, by increasing the permeate flow rate, the resulted permeate temperature is reduced in order to equalize these amounts of heat in the hot side of the heat exchanger.

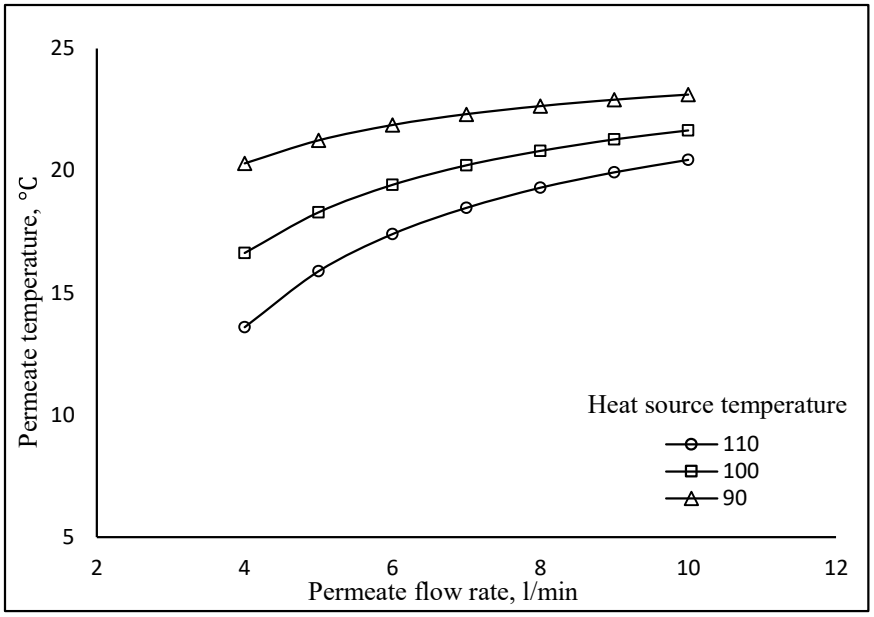

Figure 5. 9 : The permeate flow rate vs. permeate temperature, at 25 % bypass percentage and different heat source temperatures.

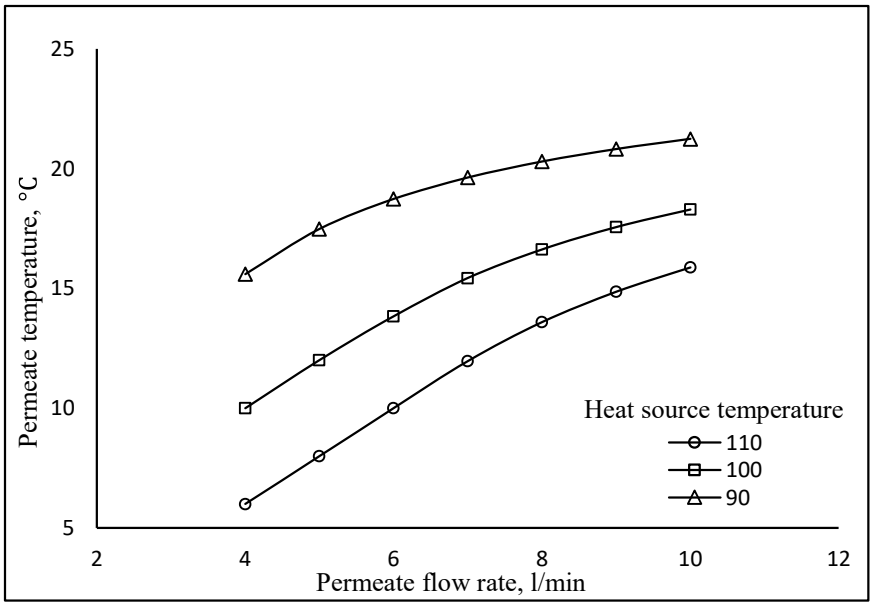

Figure 5. 10 : The permeate flow rate vs. permeate temperature, at 50 % bypass percentage and different heat source temperatures.

Fig. 5.11 shows the permeate flux obtained from the integrated system as a function of heat source temperature and bypass percentage. For 25% bypass percentage, as the input temperature increases, there is a significant increase in fresh water productivity to reach the maximum value of almost 118 kg/m^2-hr. The same trends are observed for 50 % and 75 % bypass percentages. The maximum values recorded are 125 and 133 kg/m^2-hr for 50 % and 75 %, respectively.

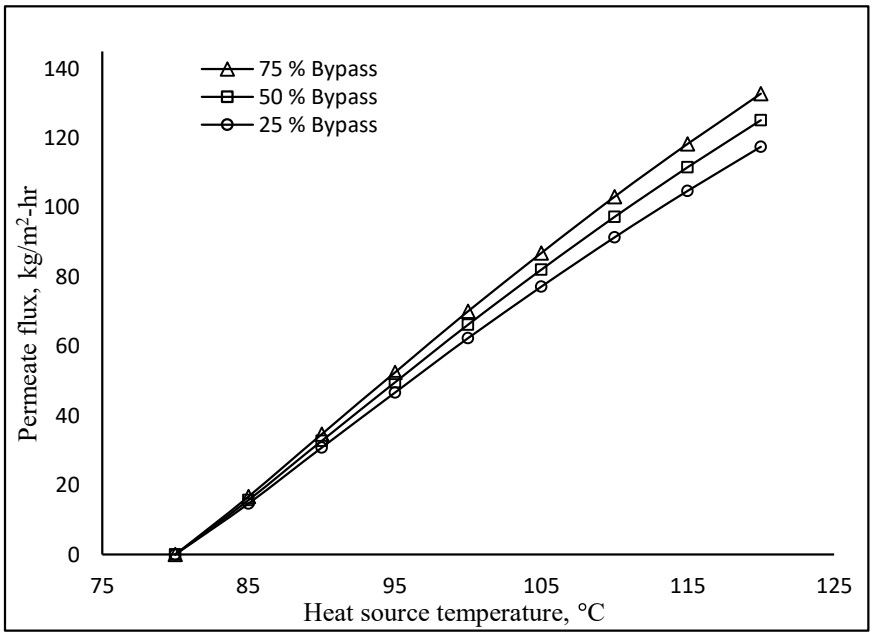

Figure 5. 11 : Effect of heat source temperature on fresh water productivity at different bypass percentages. Feed flow rate = 6 l/min and permeate flow rate = 12 l/min.

Fig. 5.12 shows the effect of heat source temperature and bypass percentage on cooling effect produced from the integrated system. At a certain bypass percentage, as the input temperature increases, the cooling effect produced is also increased similar to the behavior discussed in Fig. 3.8. The maximum values recorded for cooling effect produced are 19.5 9.8 and 2.5 kW for 25, 50 and 75 bypass percentages, respectively.

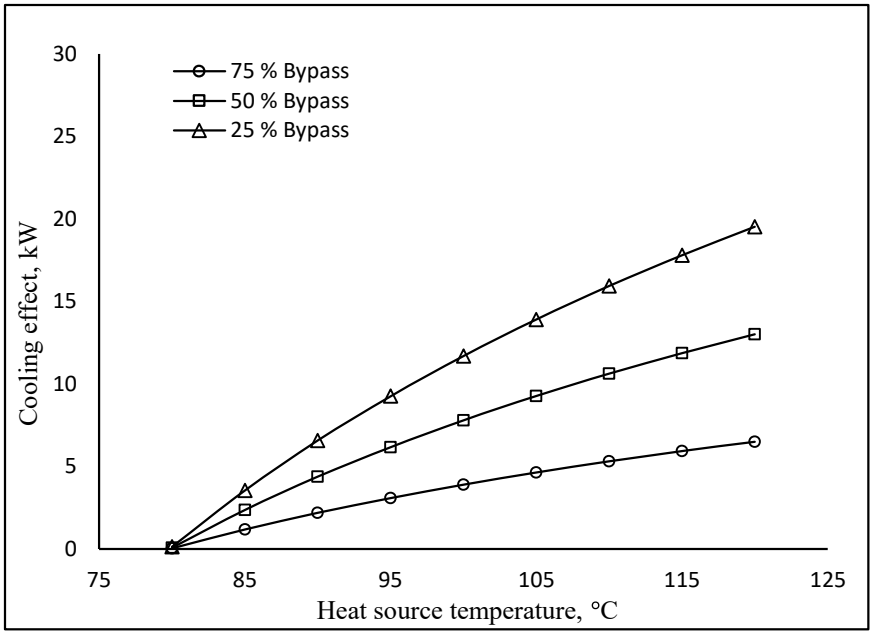

Figure 5. 12 : Effect of heat source temperature on produced cooling effect at different bypass percentages.

Fig. 5.13 shows the performance of the overall integrated system as a function of heat source temperature and bypass percentage. For 25% bypass percentage, as the input temperature increases, there is a significant increase in overall efficiency up to 0.52, followed by a slower rate of increment up to 0.57 to reach the maximum value around 0.59. The same trends are observed for 50 % and 75 % bypass percentages. The maximum values recorded are 0.4 and 0.21 for 50 % and 75 %, respectively.

This decrease in the overall system efficiency with the bypass percentages is due to the increase in the chilled water flow rate that feeds the DCMD unit to increase the fresh water productivity. This increase in chilled water branch results in a decrease in the cooling effect obtained. Therefore, from the overall efficiency definition, the rate of decrease in the cooling effect is higher than the increase in fresh water productivity and hence the overall

efficiency is decreased. This is left to the designer or the user to identify his priority; either to get more fresh water or higher cooling effect.

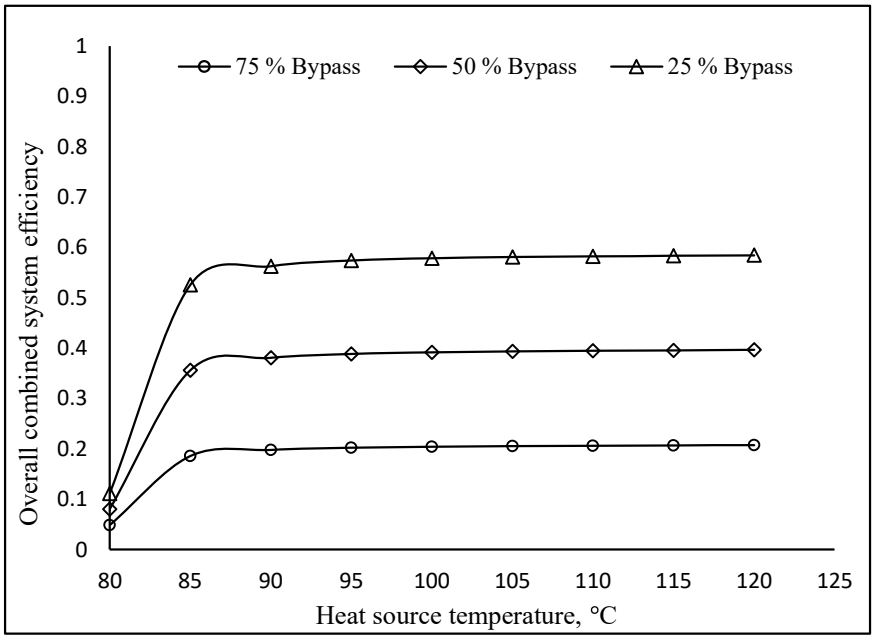

Figure 5. 13 : Effect of heat source temperature on overall integrated system efficiency. Feed flow rate = 6 l/min and permeate flow rate = 12 l/min.

5.2.3 Arrangement (C)

In this arrangement, the solar absorption cooling system solely utilized for increasing the fresh water productivity of DCMD system. The effect of heat source temperature on fresh water productivity, cooling capacity and overall integrated system performance is studied over a range of temperatures from 80 °C to 120 °C with an increment of 10 °C. In this configuration, the chilled water ($\dot{m}_{17}$) that is produced from evaporator is totally introduced to coolant heat exchanger (CHX), refer to Fig. 5.4.

For DCMD system, certain assumptions have been considered for flow conditions. The feed flow rate (cooling water), represented by ($\dot{m}_{15}$), that is introduced to the feed heat exchanger (FHX) at 25 °C is assumed to be at a rate of 6 l/min, at each selected heat source

temperature. The permeate flow rate, represented by ($\dot{m}_{19}$), that is introduced to coolant heat exchanger (CHX) at 25 °C is varied from 4 l/min to 10 l/min, at each selected heat source temperature. Figs. 5.14 and 5.15 report the results of this analysis.

Fig. 5.14 shows permeate flow rate vs. permeate temperature at different heat source temperatures. It can be seen clearly that, at a certain heat source temperature, increasing the permeate flow rate ($\dot{m}_{19}$) through the coolant heat exchanger results in an increase in the permeate temperature (T_{19}) that introduced to DCMD unit. This is because, for instance at 90 °C heat source temperature, a certain heat transfer rate is resulted in the cold side of CHX.

Therefore, by increasing the permeate flow rate, the resulted permeate temperature is reduced in order to equalize these amounts of heat in the hot side of the heat exchanger. Similarly, the same behavior is observed upon increasing the heat source temperature from 90 °C to 120 °C.

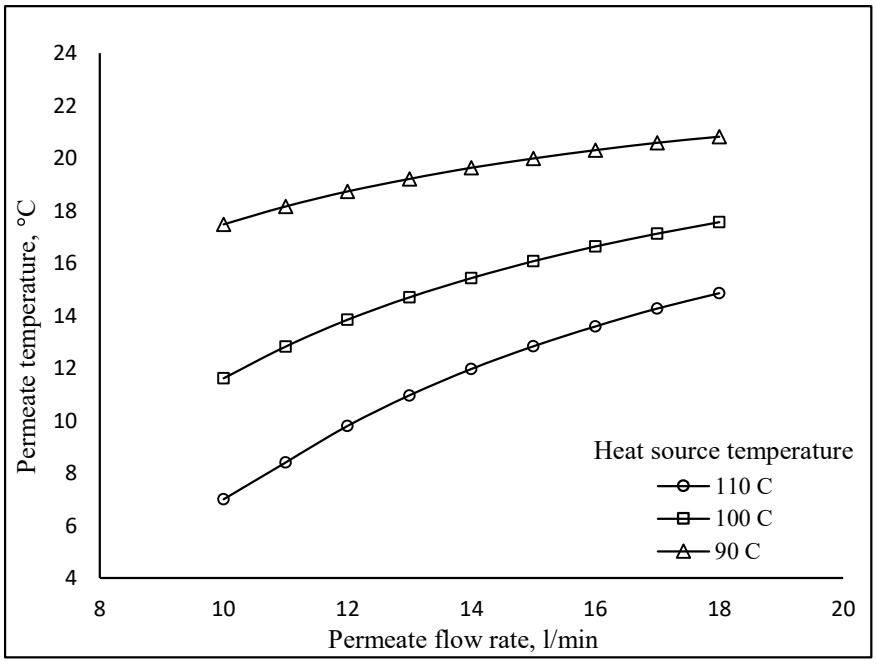

Figure 5. 14 : Permeate flow rate vs. permeate temperature at different heat source temperatures

Fig. 5.15 shows the effect of heat source temperature on permeate flux obtained. As the heat source temperature increased, the fresh water produced is also increased similar to the behavior illustrated in Fig. 5.6. The maximum flux obtained from this configuration is almost closed to 140 kg/m^2-hr. The flow condition (in DCMD) is 6 l/min and 12 l/min for feed and permeate flow rates, respectively.

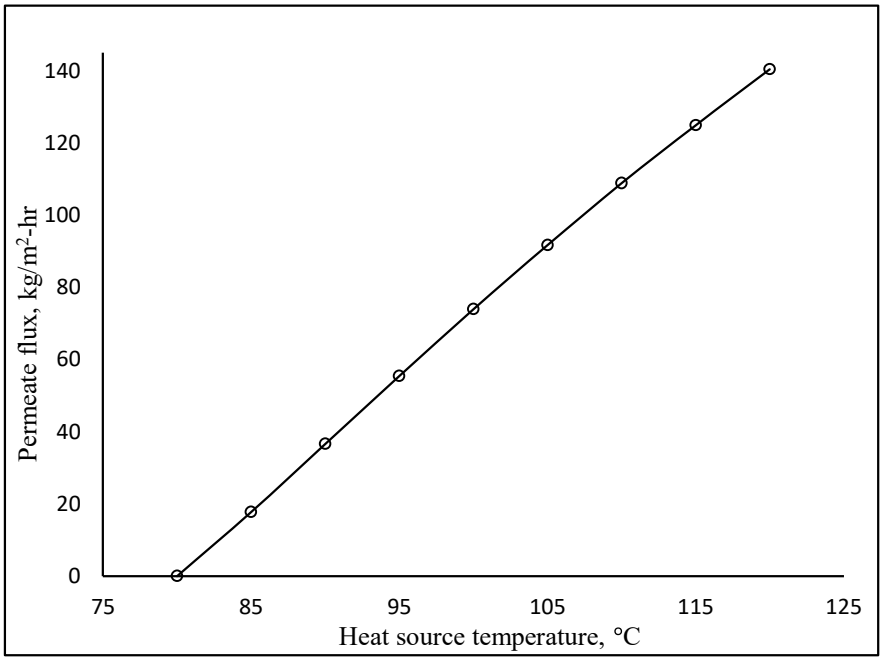

Figure 5. 15 : Effect of heat source temperature on fresh water productivity at different bypass percentages. Feed flow rate = 6 l/min and permeate flow rate = 12 l/min.

5.2.4 Comparison between integrated system arrangements

In this section, a comparison between the three mentioned arrangements for the integrated solar absorption cooling and membrane distillation system is presented. The comparison is based on the cooling effect and fresh water obtained from each configuration.

Fig. 5.16 shows the heat source temperature vs. cooling effect obtained from different arrangements. It can be seen clearly that, increasing the heat source temperature results in an increase in the cooling effect obtained. Configuration (A) appears as the best choice for

providing a cooling effect that starting from almost 0.2 kW at 80 °C and reach up to 26 kW for 120 °C heat source temperature. Then followed by configuration (B) with 25 %, 50 % and 75 % bypass percentages with maximum cooling effect obtained as 19.5, 9.8 and 2.5 Kw, respectively. Note that, configuration (C) has no cooling effect because it is totally utilized for DCMD productivity improvement.

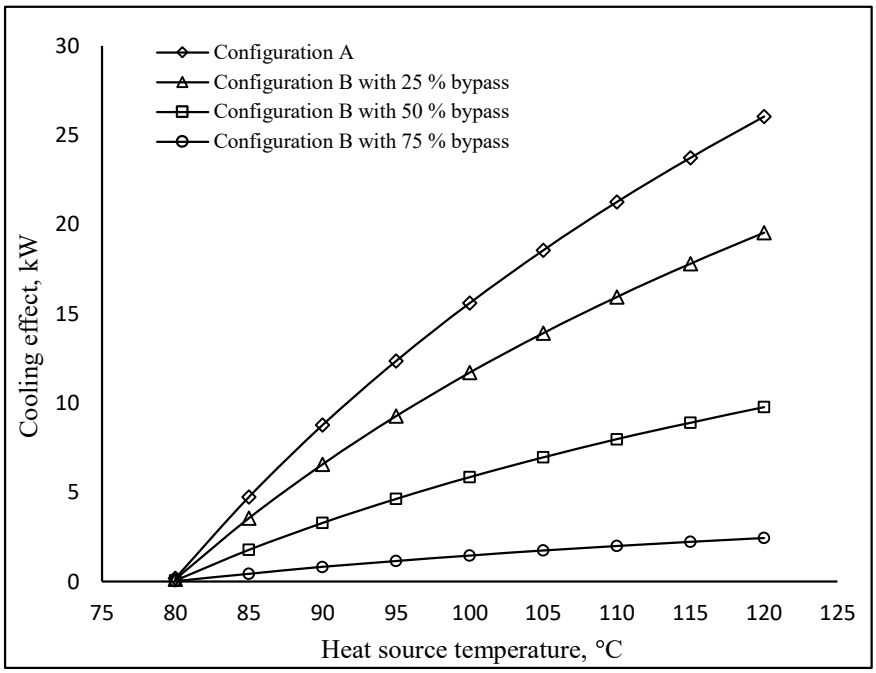

Figure 5. 16 : Heat source temperature vs. cooling effect produced from different integrated system configurations

Fig. 5.17 compares the fresh water productivity for different integrated system arrangements. As the heat source temperature increases, the fresh water produced from each configuration is also increased. As shown in the figure, configuration (C) has the best performance in term of water productivity which can reach up to 140 kg/m^2-hr at 120 °C heat source temperature. Then followed by configuration (B) with 75 %, 50 % 25 % and configuration (A). The maximum flux obtained are 133, 125, 118 and 110 kg/m^2-hr, respectively.

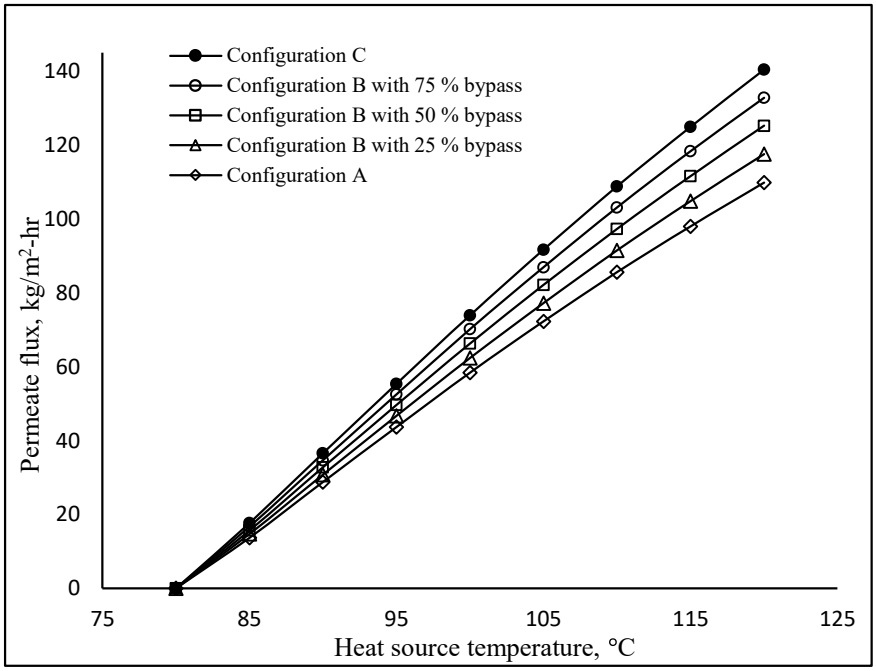

Figure 5. 17 : Heat source temperature vs. permeate flux obtained from different integrated system configurations. Feed flow rate = 6 l/min and permeate flow rate = 12 l/min.

CHAPTER 6

COST ANALYSIS

6.1 Life Cycle Cost Analyses of Solar Absorption Cooling System

In this section, the life cycle cost analysis (LCCA) of solar absorption air conditioning system is presented. The LCCA is the estimation of the total cost of a system throughout its life time. The life cycle cost analysis (LCCA) is based on present worth cost (PWC) method which is the useful tool to merit various cooling systems for building applications.

The total present worth value for any analysis is determined by summing the present worth value so fall individual items under consideration, both future single payment (i.e., replacement cost) items and series of equal future payments (i.e., annual operating cost). The cost or the value of money is a function of the available interest rate and inflation rate. The following sections present details of how the various costs are evaluated [65].

6.1.1 Initial costs

The initial costs of the solar absorption cooling system include absorption chiller, solar energy collection system and solution pump. The initial cost therefore should include, in addition to the purchase and installation of the system, the various subsystems necessary for effective operation. This includes piping, wiring and specific structures.

The solar energy collection system plays the most significant role in the initial cost of the solar absorption cooling system. The price of a evacuated tube solar collector is $371/m^2$ [65]. For higher temperature, which will be needed for the double-effect absorption system, parabolic troughs may have to be used. The cost of these would be higher than for flat-plate collectors. However, as a result of the higher temperatures achieved, the surface area required would be smaller which may help to offset the extra cost.

6.1.2 Operating costs

Operating costs, which include the costs of electricity, wages of employees, supplies, water and materials, are those incurred by the actual operation of the system. Annual operating hours for solar absorption system is 2555 (6 hours per day). The operating costs of solar absorption system is mainly depending upon the unit cost of electricity. The unit cost of electricity in Saudi Arabia is $ 0.13 per kWh [66].

6.1.3 Maintenance costs

Solar absorption cooling systems are more reliable and have lower maintenance costs because they have fewer highly stressed moving parts [67]. The maintenance costs of absorption cooling systems are labor and material expense required to maintain system in suitable use condition. There are various levels of maintenance that may be applied to building air conditioning services. The three most common levels are run to failure (unsuitable for the hospital), preventive, and finally predictive maintenance [67]. The maintenance cost is difficult to quantify because it depends on a large number of variables such as local labor rates, their experience, the age of the system, length of time of operation,

etc. Maintenance costs cited in various studies show that the absorption cooling system's maintenance costs range from 1- 2 % of the total capital costs [65].

6.1.4 Replacement costs

The replacement costs include the costs of auxiliary equipments that needs to be replaced during the project life time. For solar absorption cooling system, the cost of solar collector array and solution pump is not included in the replacement cost because the life time of the solar array and the pump are same as analysis period.

6.1.5 Salvage values

The salvage value of solar absorption system is the estimated value of the system at the end of the useful life. Hence, the salvage value of the system after life time is estimated by assuming 5 % of the total initial costs of each system [65].

Thereafter, the life cycle cost using PWC method is calculated using the following equation [65]:

$$LCCA = C_A + AC_O + AC_M + BC_R - BC_S \quad (6.1)$$

Where C_A, C_O, C_M, C_R and C_S are the initial, operating, maintenance, replacement costs and salvage value, respectively.

The following equations is used to calculate the constants A and B, where *i* and *n* are the discount rate and project life time, respectively [65]:

$$A = \left[\frac{(1+i)^n - 1}{i\,(1+i)^n}\right] \quad (6.2)$$

$$B = \left[\frac{1}{(1+i)^n}\right] \quad (6.3)$$

6.2 Life Cycle Cost Analyses of DCMD System

In this section, the cost analysis of direct contact membrane system (DCMD) is presented. Economics in the MD process for desalination and water purification is based on technical factors such as energy source, plant capacity, salinity, and design features. Among these factors, energy requirement for the process has an important effect on the overall process economics. Thermal and electrical energy is required for the MD process. Hence, the consumption of high thermal energy in the MD process is a barrier for the commercialization in the industry.

Since MD requires lower operating temperatures than the conventional distillation processes, it is possible to utilize low-grade energy sources from industrial processes. This is expected to lead to significant savings in the operating costs, which in turn will result in more affordable product. The following sections present details of how the various costs are evaluated.

6.2.1 Capital Costs

The total capital costs divided into direct and indirect capital costs. The indirect capital cost can be represented as 10 % of the direct capital costs. The direct capital costs can be evaluated as the summation of the following costs [68]:

- Total cost of membrane module ($)
- Cost of heat exchangers ($) = heat exchanger area (m^2) * cost per unit area ($/$m^2$)

Then, the heat to be provided by the heat exchangers and required heat exchangers area are presented in the following equations [68]:

$$Q = \dot{m}_f * C_{pf} * (T_{out} - T_{in}) \quad (6.4)$$

$$A = Q / U \Delta T \quad (6.5)$$

Where $\dot{m}_f$, C_{pf}, T_{out} and T_{in} are the mass flow rate of transferable fluid, specific heat of transferable fluid, inlet and exit temperature, respectively.

Also, U and ΔT are the global heat transfer coefficient and the average temperature difference through heat exchanger, respectively.

Finally, the annual fixed charges are determined as [68], where *W* and *f* are the annual system capacity in (m^3/day) and system availability:

- Annual fixed charges ($) = *a* * total capital costs / (*f* * *W* * *365*)

6.2.2 Operation and Maintenance Costs

The annual operation and maintenance costs are evaluated by considering the following costs [68]:

- Membrane replacement ($/year) = 3 times * total membrane module costs
- Cost of chemicals ($/year) = specific chemical cost ($/$m^3$) * (*W* * 365 * *f*)
- Cost of spares ($/year) = specific spares cost ($/$m^3$) * (*W* * 365 * *f*)
- Cost of labour ($/year) = specific labour cost ($/$m^3$) * (*W* * 365 * *f*)
- Brine disposal ($/year) = specific brine disposal cost ($/$m^3$) * (*W* * 365 * *f*)

Finally, the annual operation and maintenance charges are determined as [68]:

- Annual O&M charges ($) = total annual O$M cost/ (*f* * *W* * *365*)

6.3 Case Study

In order to perform an economic analysis on the proposed integrated solar cooling and desalination system, a case study is considered for one of the system arrangements. So, considering arrangement (B) with 50 % bypass percentage working at 100 °C heat source temperature. The solar absorption cooling (SAC) system capacity in this case is 15.6 kW. The solar collection system is considered as evacuated tube solar collectors with total area of 80 m^2. The required initial costs of SAC system and solar collector array is presented in Table 6.1.

Table 6. 1 : Initial costs of solar absorption system

Components	Estimated Specific Cost	Life Time [69] (Years)
Absorption Chiller	195 $/kW [67]	20
Solar Collector Array	371 $/$m^2$ [65]	20

For DCMD system, the hot feed (6 l/min) enters the feed heat exchanger (FHX) at 25 °C and leaves at 65 °C. For permeate side, the permeate (4.5 l/min) enters the coolant heat exchanger (CHX) at °C and leaves at 10 °C. This configuration is able to produce 58.6 m^3/day as fresh water. In addition, in order to conduct cost analysis for DCMD system, the following information and assumption are used as presented in Table 6.2.

Table 6. 2 : Data and assumptions used in DCMD economical study

Plant availability (*f*)	90%
Plant capacity (*W*)	58.6 m^3/day
Amortization factor (*a*)	0.08
Spares cost	\$0.033/m^3 [68]
Labor cost	\$0.03/m^3 [68]
Chemical cost	\$0.018/m^3 [68]
Brine disposal	\$0.0015/m^3 [68]
Heat exchangers cost	\$1540/m^2 [68]

Table 6. 3 : Calculated life cycle cost items form integrated SAC-DCMD

	Description	Costs
1	**Capital cost (C_A)**	
	- **Absorption Chiller (SAC)**	
	= 15.6 (kW) * 195 ($/kW)	$3042
	- **Solar Collector Array (SAC)**	
	= 80 (m^2) * 371 ($/$m^2$)	$29680
	- **Cost of Membrane Module (DCMD)**	$100
	- **Cost of Feed Heat Exchanger (DCMD)**	
	= 0.1 (m^2) * 1540 ($/$m^2$)	$154
	- **Cost of Coolant Heat Exchanger (DCMD)**	
	= 0.095 (m^2) * 1540 ($/$m^2$)	$146.3
	- **Indirect Capital Costs (DCMD)**	
	= 0.1 * (100 + 154 + 146.3)	$40.03
7	**Maintenance Cost (C_M)**	
	- **Maintenance Cost (SAC)**	
	= 0.01 * 32722	$327.22
	- **Spares Cost (DCMD)**	
	= 0.033 ($/$m^3$) * 58.6 * 365 * 0.9	$635.3
	- **Labor Cost (DCMD)**	
	= 0.03 ($/$m^3$) * 58.6 * 365 * 0.9	$577.5
8	**Operating Cost (C_O)**	
	- **Chemicals Cost (DCMD)**	
	= 0.018 ($/$m^3$) * 58.6 * 365 * 0.9	$346.5
	- **Module Replacement Cost (DCMD)**	
	= 3 * $100	$300
	- **Brine Disposal Cost (DCMD)**	
	= 0.0015 ($/$m^3$) * 58.6 * 365 * 0.9	$28.88
9	**Replacement Cost (C_{RE})**	_
10	**Salvage Value (C_S)**	
	- **Salvage Value (SAC)**	
	= 0.05 * 32722	$1636.1

6.3.1 Life Cycle Cost Analysis (LCCA)

In this section, the annual costs for integrated SAC-DCMD system are presented in the following cash flow diagram:

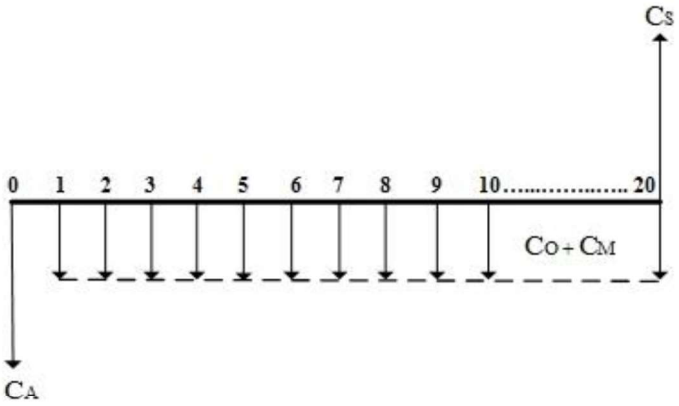

Figure 6. 1 : Cash flow diagram for integrated SAC-DCMD

C_A (capital cost) = \$33162.33

C_O (operating cost) = \$675.38

C_M (maintenance cost) = \$1540.02

C_{RE} (replacement cost) = \$0

C_S (salvage value) = \$1636.1

Then, the total life cycle cost can be determined using equations 6.1 to 6.3 assuming discount rate (i) and life time (n) as 5 % and 20 years:

$$A = \left[\frac{(1+i)^n-1}{i\,(1+i)^n}\right] = \left[\frac{(1+0.05)^{20}-1}{0.05\,(1+0.05)^{20}}\right] = 12.46$$

$$B = \left[\frac{1}{(1+i)^n}\right] = \left[\frac{1}{(1+0.05)^{20}}\right] = 0.377$$

$$LCCA = C_A + AC_O + AC_M + BC_R - BC_S$$

LCCA = \$33162.33 + (12.46*\$675.38) + (12.46*\$1540.02) + (0.377*\$0) – (0.377*\$1636.1) = \$60150

6.3.2 DCMD System Unit Cost

In this section, the unit cost for the direct contact membrane distillation (DCMD) system is calculated as:

- Annual fixed charges ($/m^3) = 0.08 * ($400.3 + $40.03) / (0.9*58.6*365) = 0.002
- Annual O&M charges ($/m^3) = $1888.18 / (0.9*58.6*365) = 0.1
- The total unit cost ($/m^3) = 0.002 + 0.1 = 0.102 $/m^3

CHAPTER 7

CONCLUSION AND RECOMMENDATIONS

In this work, an integrated solar cooling and thermal desalination system was investigated. The system is broadly based on solar driven, single effect lithium bromide-water absorption cycle and a direct contact membrane distillation system. The energy required to drive the system is provided by means of evacuated tube solar collectors. The combined system based on LiBr-water absorption cycle and DCMD unit is determined to be a best-suited choice for the system design. It is because of the simplicity in design as well as high flux rate of DCMD system. The suggested system is aimed to have simultaneous production of cooling effect as well as fresh water for typical family house in Dhahran, Saudi Arabia.

In order to come up with an integrated model, a steady state models for solar LiBr-water absorption cooling cycle and direct contact membrane distillation unit is developed. The following studies are conducted using the developed integrated model to compute the steady state performance of the integrated system.

- Steady state operation analysis for both absorption and DCMD sub-systems
- System response to the increase in the heat gain temperature
- System response to the increase in the LiBr-water solution flow rate
- System response to the increase in the outside cooling seawater flow rate
- System response to the decrease in the house cooling load (off season)

First, an evaporator cooling capacity of 20 kW was considered as a case study and all temperatures, masses and heat transfer rates were obtained during a steady state operation. Thermal masses and temperatures of the external loops were included in the computation of system design. To study the system performance, heat gain temperature was varied along with all system parameters. The generator heat transfer rate increases rapidly, followed by the absorber heat transfer rate, the condenser and evaporator heat transfer rates, respectively. The trends observed for system flow rates and COP are shown to be the same. The steady-state performance results obtained using the developed model are compared with an equivalent steady-state model, and the parameters such as condenser heat transfer rate, flow rates and COP are found to match closely. A maximum deviation of 2.44% is observed in the condenser heat transfer rate estimation upon validating it with the results obtained using TRNSYS program (Balghouthi et al., 2008) for the same cooling capacity of 11 kW.

Second, steady state analysis for direct contact membrane distillation is conducted assuming several membrane properties and geometrical constants. The effect of variation in various parameters such as feed and coolant flow rates and temperatures on system performance are studied. First, a 10 °C step-increase and 10 °C step-decrease in the feed and coolant temperatures are considered, respectively, whereas three different values for feed and coolant flow rates are assumed. The results observed indicate that the permeate flux increases rapidly with increasing feed temperature, feed and coolant flow rates, whereas decreasing trends are obtained with increasing the coolant temperature. After validating the developed model with another steady-state model under the same operating

conditions, results obtained are found to match closely. A maximum deviation of 9% is observed in the effect of feed temperature.

Third, after the thermodynamic models are conducted for both solar cooling and thermal desalination sub-systems, two configurations for proposed integrated system are suggested and designed. Configuration (A) is aimed to obtain simultaneous production for both cooling effect as well as fresh water needs where the desalination unit is driven by the rejected cooling water and coolant water for feed and cold sides, respectively. Moreover, configuration (B) is aimed to improve the fresh water productivity of the desalination unit when the cooling load has a low demand. In this configuration, the desalination unit is driven by rejected cooling water and obtained chilled water for both feed and cold sides, respectively. A steady state modeling for the proposed configurations are also conducted.

Fourth, different arrangements for the proposed integrated system are presented. The effect of the variation in heat source temperature, feed and permeate flow rates on overall system efficiency, cooling effect and obtained permeate flux are studied. The results observed indicate that the cooling capacity, permeate flux and overall system performance show some increasing trends when the heat source temperature is increased. Additionally, the results show that when the feed flow rate is increased, the permeate flux is decreased whereas the cooling capacity do not show any influence with feed flow rate variation. However, configuration (C) appears to be the best arrangement in term of water productivity while configuration (A) is the best in terms of cooling effect and overall system performance.

Since the research in solar driven lithium bromide-water vapor absorption cooling system is ongoing, it is recommended for a 24 hours operating system to undergo a detailed design and analysis for solar collectors field as well as the heat storage systems. Furthermore, for heat transfer coefficients, constant values were used in the developed model. Appropriate correlations could be used to estimate the exact values for heat transfer coefficient to model the mass and heat transfer processes more accurately. The present model assumes steady state mass and heat transfer processes inside the generator of the absorption system. Future models based on the outcome of this study, it is also recommended to take into consideration the transient phenomena by considering the solar gain at each time instance.

REFERENCES

[1] "Muhammad Umar Siddiqui, Development of a continuously operated solar powered refrigeration system", Master Thesis, King Fahad University of Petroleum and Minerals, 2011.

[2] G. Rao, "Direct-Contact Membrane Distillation : Simplified Flux Prediction , Mass Transfer Mechanisms , and Membrane Cleaning," no. August, 2014.

[3] B. L. Pangarkar, S. K. Deshmukh, V. S. Sapkal, and R. S. Sapkal, "Review of membrane distillation process for water purification," *Desalin. Water Treat.*, vol. 3994, no. November, pp. 1–23, 2014.

[4] L. Martínez and F. J. Florido-Díaz, "Theoretical and experimental studies on desalination using membrane distillation," *Desalination*, vol. 139, no. 1–3, pp. 373–379, 2001.

[5] V. Calabrò, B. L. Jiao, and E. Drioli, "Theoretical and experimental study on membrane distillation in the concentration of orange juice," *Ind. Eng. Chem. Res.*, vol. 33, no. 7, pp. 1803–1808, 1994.

[6] K. W. Lawson and D. R. Lloyd, "Membrane distillation. I. Module design and performance evaluation using vacuum membrane distillation," *J. Memb. Sci.*, vol. 120, no. 1, pp. 111–121, 1996.

[7] A. S. Jönsson, R. Wimmerstedt, and A. C. Harrysson, "Membrane distillation - a theoretical study of evaporation through microporous membranes," *Desalination*, vol. 56, no. C, pp. 237–249, 1985.

[8] L. Basini, G. D'Angelo, M. Gobbi, G. C. Sarti, and C. Gostoli, "A desalination process through sweeping gas membrane distillation," *Desalination*, vol. 64, no. C, pp. 245–257, 1987.

[9] M. Khayet, P. Godino, and J. I. Mengual, "Theory and experiments on sweeping gas membrane distillation," *J. Memb. Sci.*, vol. 165, no. 2, pp. 261–272, 2000.

[10] M. Khayet, P. Godino, and J. I. Mengual, "Nature of flow on sweeping gas membrane distillation," *J. Memb. Sci.*, vol. 170, no. 2, pp. 243–255, 2000.

[11] S. Bandini, C. Gostoli, and G. C. Sarti, "Separation efficiency in vacuum membrane distillation," *J. Memb. Sci.*, vol. 73, no. 2–3, pp. 217–229, 1992.

[12] G. C. Sarti, C. Gostoli, and S. Bandini, "Extraction of organic components from aqueous streams by vacuum membrane distillation," *J. Memb. Sci.*, vol. 80, no. 1, pp. 21–33, 1993.

[13] "PERFORMANCE OF A SOLAR LiBr-WATER ABSORPTION REFRIGERATION SYSTEM," vol. 2, no. 3, pp. 275–282, 1992.

[14] O. Marc, G. Anies, F. Lucas, and J. Castaing-Lasvignottes, "Assessing performance and controlling operating conditions of a solar driven absorption chiller using

simplified numerical models," *Sol. Energy*, vol. 86, no. 9, pp. 2231–2239, 2012.

[15] D. S. Ayou, J. C. Bruno, and A. Coronas, "ScienceDirect Modelling , simulation and analysis of solar absorption power-cooling systems Mode ` mes e ´ lectriques fonctionnant gra ` l ' absorption solaire ˆ ce a syste," vol. 9, 2013.

[16] Z. Y. Xu, R. Z. Wang, and H. B. Wang, "Experimental evaluation of a variable effect LiBr – water absorption chiller designed for high-efficient solar cooling system Evaluation expérimentale d ' un refroidisseur à absorption LiBr-eau à effet variable pour un système de froid solaire à efficacit," vol. 59, pp. 135–143, 2015.

[17] B. Bakhtiari, L. Fradette, R. Legros, and J. Paris, "A model for analysis and design of H 2 O – LiBr absorption heat pumps," *Energy Convers. Manag.*, vol. 52, no. 2, pp. 1439–1448, 2011.

[18] A. Pongtornkulpanich, S. Thepa, M. Amornkitbamrung, and C. Butcher, "Experience with fully operational solar-driven 10-ton LiBr / H 2 O single-effect absorption cooling system in Thailand," vol. 33, pp. 943–949, 2008.

[19] A. Lecuona, R. Ventas, C. Vereda, and R. López, "Absorption solar cooling systems using optimal driving temperatures," *Appl. Therm. Eng.*, vol. 79, pp. 140–148, 2015.

[20] J. Muye, D. S. Ayou, R. Saravanan, and A. Coronas, "Performance study of a solar absorption power-cooling system," *Appl. Therm. Eng.*, 2015.

[21] C. D. Ho, C. H. Huang, F. C. Tsai, and W. T. Chen, "Performance improvement on distillate flux of countercurrent-flow direct contact membrane distillation systems," *Desalination*, vol. 338, no. 1, pp. 26–32, 2014.

[22] L. Martínez and J. M. Rodríguez-Maroto, "Effects of membrane and module design improvements on flux in direct contact membrane distillation," *Desalination*, vol. 205, no. 1–3, pp. 97–103, 2007.

[23] A. Khalifa, H. Ahmad, M. Antar, T. Laoui, and M. Khayet, "Experimental and Theoretical Investigations on Water Desalination Using Direct Contact Membrane Distillation," pp. 1–27.

[24] M. Khayet, T. Matsuura, J. I. Mengual, and M. Qtaishat, "Design of novel direct contact membrane distillation membranes," vol. 192, no. August 2005, pp. 105–111, 2006.

[25] Y. Yun, R. Ma, W. Zhang, A. G. Fane, and J. Li, "Direct contact membrane distillation mechanism for high concentration NaCl solutions," vol. 188, no. February 2005, pp. 251–262, 2006.

[26] P. Termpiyakul and R. Jiraratananon, "Heat and mass transfer characteristics of a direct contact membrane distillation process for desalination," vol. 177, pp. 133–141, 2005.

[27] L. Mart and J. M. Rodr, "On transport resistances in direct contact membrane distillation," vol. 295, pp. 28–39, 2007.

[28] Z. Ding, R. Ma, and A. G. Faneb, "A new model for mass transfer in direct contact

membrane distillation," vol. 9164, 2002.

[29] L. Martinez and F. Florido-Diaz, "Theoretical and experimental studies on desalination using membrane distillation," *Desalination*, vol. 139, no. May, pp. 373–379, 2001.

[30] F. Laganà, G. Barbieri, and E. Drioli, "Direct contact membrane distillation: Modelling and concentration experiments," *J. Memb. Sci.*, vol. 166, no. 1, pp. 1–11, 2000.

[31] D. U. Lawal and A. E. Khalifa, "Theoretical and Statistical Models for Predicting Flux in Direct Contact Membrane Distillation," vol. 4, no. 8, pp. 124–135, 2014.

[32] V. V Slesarenko, "Heat pumps as a source o f heat energy for desalination o f seawater," vol. 139, no. May, pp. 405–410, 2001.

[33] G. Franchini, A. Perdichizzi, and A. Picinardi, "HD desalination by heat rejected from solar cooling systems," *2010 IEEE Int. Energy Conf. Exhib. EnergyCon 2010*, pp. 63–68, 2010.

[34] D. Alarcón-padilla and L. García-rodríguez, "Application of absorption heat pumps to multi-effect distillation : a case study of solar desalination," vol. 212, pp. 294–302, 2007.

[35] F. Mandani, H. Ettouney, and H. El-Dessouky, "LiBr-H2O absorption heat pump for single-effect evaporation desalination process," *Desalination*, vol. 128, pp. 161–176, 2000.

[36] G. Yuan, L. Zhang, and H. Zhang, "Experimental research of an integrative unit for air-conditioning and desalination," *Desalination*, vol. 182, no. 1–3, pp. 511–516, 2005.

[37] V. G. Gude and N. Nirmalakhandan, "Combined desalination and solar-assisted air-conditioning system," *Energy Convers. Manag.*, vol. 49, no. 11, pp. 3326–3330, 2008.

[38] D. C. Alarcón-Padilla, L. García-Rodríguez, and J. Blanco-Gálvez, "Design recommendations for a multi-effect distillation plant connected to a double-effect absorption heat pump: A solar desalination case study," *Desalination*, vol. 262, no. 1–3, pp. 11–14, 2010.

[39] Y. Wang and N. Lior, "Proposal and analysis of a high-efficiency combined desalination and refrigeration system based on the LiBr–H2O absorption cycle—Part 1: System configuration and mathematical model," *Energy Convers. Manag.*, vol. 52, no. 1, pp. 220–227, 2011.

[40] Y. Wang and N. Lior, "Thermoeconomic analysis of a low-temperature multi-effect thermal desalination system coupled with an absorption heat pump," *Energy*, vol. 36, no. 6, pp. 3878–3887, 2011.

[41] K. Ghali, N. Ghaddar, and A. Alsaidi, "Experimental and Theoretical Study of an Optimized Integrated Solar Desalination and Air Conditioning Unit," *Int. J. Green Energy*, vol. 8, no. 1, pp. 81–99, 2011.

[42] Z. S. Abdel-Rehim and A. Lashine, “A Study of Solar Desalination Still Combined with Air-Conditioning System,” *ISRN Renew. Energy*, vol. 2012, pp. 1–7, 2012.

[43] H. K. Abdulrahim and M. A. Darwish, “Thermal desalination and air conditioning using absorption cycle,” *Desalin. Water Treat.*, vol. 55, no. 12, pp. 3310–3329, 2015.

[44] C. Chiranjeevi and T. Srinivas, “Combined two stage desalination and cooling plant,” *Desalination*, vol. 345, pp. 56–63, 2014.

[45] S. A. Nada, H. F. Elattar, and A. Fouda, “Experimental study for hybrid humidification–dehumidification water desalination and air conditioning system,” *Desalination*, vol. 363, pp. 112–125, 2015.

[46] S. A. Nada, H. F. Elattar, and A. Fouda, “Performance analysis of proposed hybrid air conditioning and humidification–dehumidification systems for energy saving and water production in hot and dry climatic regions,” *Energy Convers. Manag.*, vol. 96, pp. 208–227, 2015.

[47] “Theoretical Study of a Solar Powered Absoprtion / MED Combined System,” vol. 82, p. 1991, 1991.

[48] P. Taylor, H. K. Abdulrahim, and M. A. Darwish, “Desalination and Water Treatment Thermal desalination and air conditioning using absorption cycle,” no. July, pp. 37–41, 2014.

[49] G. A. Florides, S. A. Kalogirou, S. A. Tassou, and L. C. Wrobel, “Modelling, simulation and warming impact assessment of a domestic-size absorption solar cooling system,” *Appl. Therm. Eng.*, vol. 22, no. 12, pp. 1313–1325, 2002.

[50] S. Klein and F. Alvarado, “Engineering equation solver,” *F-Chart Software, Box*, pp. 1–2, 2002.

[51] M. Balghouthi, M. H. Chahbani, and A. Guizani, “Feasibility of solar absorption air conditioning in Tunisia,” *Build. Environ.*, vol. 43, no. 9, pp. 1459–1470, 2008.

[52] A. Gonz??lez-Gil, M. Izquierdo, J. D. Marcos, and E. Palacios, “Experimental evaluation of a direct air-cooled lithium bromide-water absorption prototype for solar air conditioning,” *Appl. Therm. Eng.*, vol. 31, no. 16, pp. 3358–3368, 2011.

[53] M. Khayet, “Membranes and theoretical modeling of membrane distillation: A review,” *Adv. Colloid Interface Sci.*, vol. 164, no. 1–2, pp. 56–88, 2011.

[54] M. Essalhi and M. Khayet, “Self-sustained webs of polyvinylidene fluoride electrospun nanofibers at different electrospinning times: 1. Desalination by direct contact membrane distillation,” *J. Memb. Sci.*, vol. 433, pp. 167–179, 2013.

[55] Z. W. Song and L. Y. Jiang, “Optimization of morphology and perf ormance of PVDF hollow fiber for direct contact membrane distillation using experimental design,” *Chem. Eng. Sci.*, vol. 101, pp. 130–143, 2013.

[56] S. B. Iversen, V. K. Bhatia, K. Dam-Johansen, and G. Jonsson, “Characterization of microporous membranes for use in membrane contactors,” *J. Memb. Sci.*, vol. 130,

no. 1–2, pp. 205–217, 1997.

[57] Ó. Andrjesdóttir, C. L. Ong, M. Nabavi, S. Paredes, A. S. G. Khalil, B. Michel, and D. Poulikakos, “An experimentally optimized model for heat and mass transfer in direct contact membrane distillation,” *Int. J. Heat Mass Transf.*, vol. 66, pp. 855–867, 2013.

[58] A. Alkhudhiri, N. Darwish, and N. Hilal, “Membrane distillation: A comprehensive review,” *Desalination*, vol. 287, pp. 2–18, 2012.

[59] J. Phattaranawik, R. Jiraratananon, and A. G. Fane, “Effect of pore size distribution and air flux on mass transport in direct contact membrane distillation,” *J. Memb. Sci.*, vol. 215, no. 1–2, pp. 75–85, 2003.

[60] C. Liu, Y. Chen, W. Sheu, and C. Wang, “Effect of fl ow de fl ector on the fl ux improvement in direct contact membrane distillation,” vol. 253, pp. 16–21, 2010.

[61] M. Khayet and T. Matsuura, *Membrane Distillation: Principles and Applications*. 2011.

[62] S. Srisurichan, R. Jiraratananon, and A. G. Fane, “Mass transfer mechanisms and transport resistances in direct contact membrane distillation process,” *J. Memb. Sci.*, vol. 277, no. 1–2, pp. 186–194, 2006.

[63] L. Martínez-Díez and M. . Vázquez-González, “Temperature and concentration polarization in membrane distillation of aqueous salt solutions,” *J. Memb. Sci.*, vol. 156, no. 2, pp. 265–273, 1999.

[64] K. W. Lawson and D. R. Lloyd, “Membrane distillation,” *Journal of Membrane Science*, vol. 124, no. 1. pp. 1–25, 1997.

[65] S. Yongprayun, N. Ketjoy, W. Rakwichian, and S. Maneewan, “Techno-economic Analysis of a LiBr-H 2 O Solar Absorption Cooling System in Thailand,” vol. 2, no. 2, 2007.

[66] “Kingdom of Saudi Arabia Electricity Tariffs,” p. 1000, 2001.

[67] A. Elsafty, “Economical comparison between a solar- powered vapour absorption air-conditioning system and a vapour compression system in the Middle East,” vol. 25, pp. 569–583, 2002.

[68] S. Al-Obaidani, E. Curcio, F. Macedonio, G. Di Profio, H. Al-Hinai, and E. Drioli, “Potential of membrane distillation in seawater desalination: Thermal efficiency, sensitivity study and cost estimation,” *J. Memb. Sci.*, vol. 323, no. 1, pp. 85–98, 2008.

[69] R. C. Resources, “a37 Si: Owning and Operating Costs,” 2011.

VITAE

Name	Ahmed Salah Mohamed Yassen
Nationality	Sudanese
Date of Birth	10/8/1991
Email	alhadary248@yahoo.com
Mobile	+966530846643, +249912704589
Permanent Address	House No. 74, Block No. 16, Shambat Almaouna Street, Bahry Khartoum State, Sudan
Academic Background	**M.S. in Mechanical Engineering** December, 2016 King Fahad University of Petroleum & Minerals Dhahran, Saudi Arabia **B.S. in Mechanical Engineering** September, 2013 University of Khartoum Khartoum, Sudan
Publications	**Ahmed Yassen**, Mohammed A.Antar, M.A.I. El-Shaarawi and Atia Khalifa, "Integrated Solar Absorption Cooling and Membrane Distillation Systems". **Energy Conversion and Management**, 2017. (Status: Ready to submit) K. A. Khalid, M. A. Antar, **A. S. Yassen** and S. A. Salaudeen, "Experimental Investigations on the performance of a Cross Flow Air Heated Humidifier". **ASME International Mechanical Engineering Congress & Exposition (IMECE**), Vol. 6A, No. IMECE2015-50507, pp. V06AT07A049, Texas, November 13-19, 2015.